

ORIGINAL RESEARCH

Impact of Adenosine on Wavefront Propagation in Persistent Atrial Fibrillation: Insights From Global Noncontact Charge Density Mapping of the Left Atrium

Michael T. B. Pope , BM, BSc; Pawel Kuklik, PhD; Andre Briosoa e Gala , MD; Milena Leo , MD; Michael Mahmoudi, MBBS, PhD; John Paisey, DM; Timothy R. Betts , MD

BACKGROUND: Adenosine shortens action potential duration and refractoriness and provokes atrial fibrillation. This study aimed to evaluate the effect of adenosine on mechanisms of wavefront propagation during atrial fibrillation.

METHODS AND RESULTS: The study included 22 patients undergoing catheter ablation for persistent atrial fibrillation. Left atrial mapping was performed using the AcQMap charge density system before and after administration of intravenous adenosine at 1 or more of 3 time points during the procedure (before pulmonary vein isolation, after pulmonary vein isolation, and after nonpulmonary vein isolation ablation). Wave-front propagation patterns were evaluated allowing identification and quantification of localized rotational activation (LRA), localized irregular activation, and focal firing. Additional signal processing was performed to identify phase singularities and calculate global atrial fibrillation cycle length and dominant frequency. A total of 35 paired maps were analyzed. Adenosine shortened mean atrial fibrillation cycle length from 181.7 ± 14.3 to 165.1 ± 16.3 , (mean difference 16.6 ms; 95% CI, 11.3–21.9, $P < 0.0005$) and increased dominant frequency from 6.0 ± 0.7 Hz to 6.6 ± 0.8 Hz (95% CI, 0.4–0.9, $P < 0.0005$). This was associated with a 50% increase in the number of LRA occurrences (16.1 ± 7.6 – 24.2 ± 8.1 ; mean difference 8.1, 95% CI, 4.1–12, $P < 0.0005$) as well as a 20% increase in the number of phase singularities detected (30.1 ± 7.8 – 36.6 ± 9.3 ; mean difference 6.5; 95% CI, 2.6–10.0, $P = 0.002$). The percentage of left atrial surface area with LRA increased with adenosine and 42 of 70 zones (60%) with highest density of LRA coincided with high density LRA zones at baseline with only 28% stable across multiple maps.

CONCLUSIONS: Adenosine accelerates atrial fibrillation and promotes rotational activation patterns with no impact on focal activation. There is little evidence that rotational activation seen with adenosine represents promising targets for ablation aimed at sites of stable arrhythmogenic sources in the left atrium.

Key Words: AcQMap ■ adenosine ■ atrial fibrillation ■ localized rotational activation

Although pulmonary vein ectopy is widely recognized as the prevalent trigger for atrial fibrillation (AF), mechanisms responsible for maintaining AF and resulting in the progression from paroxysmal to persistent phenotypes are poorly understood. Adenosine is known to shorten atrial myocardial action potential duration and refractoriness, and its

administration may provoke AF.^{1–4} This effect is mediated by specific G-protein coupled cell surface receptors and activation of outward potassium currents.^{3,5} These are the same currents activated by cholinergic stimulation through the binding of acetylcholine to muscarinic receptors but despite the ionic basis for this effect being well recognized, the impact on the

Correspondence to: Michael T. B. Pope, BM, BSc, Research Fellow Office, Department of Cardiology, John Radcliffe Hospital, Headley Way, Oxford, OX3 9DU, United Kingdom. Email: Michael.pope@ouh.nhs.uk

Supplemental Material for this article is available at <https://www.ahajournals.org/doi/suppl/10.1161/JAHA.121.021166>

For Sources of Funding and Disclosures, see page 12.

© 2022 The Authors. Published on behalf of the American Heart Association, Inc., by Wiley. This is an open access article under the terms of the [Creative Commons Attribution-NonCommercial-NoDerivs](https://creativecommons.org/licenses/by-nc-nd/4.0/) License, which permits use and distribution in any medium, provided the original work is properly cited, the use is non-commercial and no modifications or adaptations are made.

JAHA is available at: www.ahajournals.org/journal/jaha

CLINICAL PERSPECTIVE

What Is New?

- Adenosine appears to exert a functional effect on atrial electrophysiology during atrial fibrillation resulting in an increase in rotational activation patterns throughout the left atrium that coincides with an increase in dominant frequency and shortening of whole chamber fibrillatory cycle length.
- Adenosine does not affect the number of focal firings.

What Are the Clinical Implications?

- Rotational activation during atrial fibrillation may represent the functional electrophysiological properties of the chamber rather than local “drivers.”
- There is little stability in sites of rotational activation after administration of adenosine suggesting these are poor targets for focal ablation of atrial fibrillation mechanisms.
- Caution should be exercised when interpreting data obtained during noncontact or noninvasive mapping with far field ventricular signals excluded using adenosine to achieve atrioventricular conduction block.

Nonstandard Abbreviations and Acronyms

AFCL	atrial fibrillation cycle length
LIA	localized irregular activation
LRA	localized rotational activation

properties of dynamic wavefront propagation during AF are less clear. Spatially limited dominant frequency mapping studies showed adenosine (or acetylcholine) infusion resulted in increased dominant frequency with differential effects between atrial sites potentially due to the heterogenous distribution of adenosine receptors across the atrial myocardium.^{6–8} This has been proposed as indirect evidence of high-frequency re-entry mechanisms maintaining AF and accelerated by adenosine.^{6,9} Hansen et al recently examined the effect of adenosine on AF in explanted human hearts (with and without a history of AF) and 10 patients in whom ablation confirmed “drivers” had been identified.¹⁰ However, the direct functional effect of adenosine on dynamic wavefront propagation in a broader population of patients undergoing ablation for persistent AF has not been evaluated.

The AcQMap (Acutus Medical, Carlsbad, CA, USA) noncontact mapping system allows visualization of

high-density whole chamber atrial propagation using a sampling frequency of 3125 Hz and spatial resolution of 2 mm on a 3-dimensional anatomical mesh of ≈ 3500 vertices.^{11,12} Localized patterns of AF propagation may be classified as localized rotational activation (LRA), localized irregular activation (LIA), and focal firing.¹¹ Ablation of these regions with repetitive activation patterns has produced favorable outcomes in patients with persistent AF.¹³

Adenosine is frequently used during noncontact mapping to cause transient atrioventricular block to reduce the effect of far-field ventricular signals. In this study we sought to evaluate the effect of adenosine on atrial propagation patterns in patients undergoing catheter ablation for symptomatic AF. The aim was to both further examine the mechanisms involved in AF maintenance and establish the extent to which atrial propagation is altered by adenosine thus potentially restricting the clinical utility of adenosine to aid AF mapping.

METHODS

The data that support the findings of this study are available from the corresponding author upon reasonable request.

Patients

Patients undergoing elective catheter ablation for persistent AF using the AcQMap system were included in the analysis. This included patients enrolled in parallel research studies (RECOVER-AF [Utilizing Novel Dipole Density Capabilities to Objectively Visualize the Etiology of Recurrent Atrial Fibrillation Following a Failed AF Ablation], NCT03368781; and BiMap-AF [Biatrial Global High-Density Electroanatomical Mapping of Atrial Fibrillation], NCT03812601) and undergoing both first-time and repeat procedures for recurrent AF. These studies were approved by the local ethics committee and conducted according to the principles of the Declaration of Helsinki. All patients gave written informed consent. Patients with a clinical contraindication to adenosine administration were excluded.

Activation Pattern Characterization

Activation patterns were classified using AcQTrack (Acutus Medical) to identify regions of rotational, irregular, and focal activation according to the definitions outlined next. This is an automated algorithm that tracks and evaluates conduction at every vertex of the anatomy (≈ 3500 in total) thereby removing any subjectivity from the classification and quantification of activation patterns. The distance between each vertex is ≈ 2 mm, which represents the spatial resolution.

Localized Rotational Activation

1. The LRA algorithm computes the degrees of conduction propagation around a central point by summing the angle differences of sequential conduction velocity vector directions around the central point. If the rotational angle of conduction exceeds 270 degrees, rotation is detected at the central point. An area of $\approx 300 \text{ mm}^2$ around the central point is considered.
2. To ensure smooth propagation around the central point, an r^2 of a linear fit of activation time to position around the central vertex must exceed 0.7.
3. Conduction velocity vector directions changes cannot exceed 45 degrees per position change around the vertex
4. Activation time difference around the central obstacle must be $>50 \text{ ms}$.

Localized Irregular Activation

1. The LIA algorithm computes the difference in angle between cardiac conduction entering and leaving a confined region. If the angle difference of conduction entering and leaving a confined region exceeds 90 degrees, LIA is detected.
2. An area of $\approx 200 \text{ mm}^2$ is considered a confined region
3. Wavefronts are considered to be passing through the region if the activation time differences between the border of the confined region and the central vertex would result in a conduction velocity between 0.3 m/s to 3.0 m/s.
4. Activations are grouped into entering and leaving the region based on the activation time with comparison to the central vertex. A mean conduction vector entering the region and leaving the region are then computed. Angle difference between the vector entering and leaving the region are computed and if the difference exceeds 90 degrees, LIA is detected.

Focal Activation

1. The focal activation algorithm determines whether an activation at a vertex came from a previous cardiac wavefront, or whether activation spontaneously started from the current activation. Focal activation is detected at a vertex if an activation is earlier than its neighbors' activation by at least 3 ms, and conduction spreads outward from the early activation.
2. Activations are connected as a wavefront if the time difference between the 2 activation times would produce a conduction velocity $>0.05 \text{ m/s}$.

For each activation detected at a vertex of the chamber, a disc (as illustrated in the examples in [Figure 1A](#)

through [1C](#)) is shown corresponding to the confined region in which the pattern is detected. For quantification of these activation patterns, as described in detail later, where these discs overlap at the same point in time (for example in the case of a meandering LRA), then a single occurrence is counted.

Electrophysiological Mapping Procedure

Procedures were carried out under general anesthetic in line with standard institutional practice. With the exception of amiodarone, antiarrhythmic drugs were stopped a minimum of 5 days before the procedure. Heparin boluses were administered before transseptal puncture followed by continuous heparin infusion to maintain an active clotting time $>350 \text{ s}$. A decapolar catheter (Inquiry, Abbott Medical) was inserted into the coronary sinus and the AcQMap mapping catheter was inserted into the left atrium. A circular mapping catheter (Inquiry Optima, Abbott Medical) was used to guide pulmonary vein isolation (PVI). In patients attending the procedure in sinus rhythm, AF was induced with burst pacing from the coronary sinus and only sustained AF was mapped for inclusion in the analysis (no patients demonstrated spontaneous termination after induction). A 3-dimensional ultrasound generated anatomy of the left atrium was reconstructed and electrophysiological recordings from 48 noncontact electrodes obtained using the AcQMap system as previously described.^{11,12} Recordings were taken at 1 or more of 3 time points during the procedure for each participant: before PVI (in those undergoing first-time procedures), immediately after PVI, and after nonpulmonary vein left atrial ablation. At each time point, an additional recording was obtained during the administration of a bolus of 15 mg of adenosine with pharmacological effect confirmed by the observation of transient atrioventricular conduction block and/or hypotension. Radiofrequency ablation was delivered to achieve PVI (or reisolation). Following this, additional nonpulmonary vein ablation was delivered guided by baseline AcQMap propagation maps targeting regions with highly repetitive patterns of focal firing, LIA, or LRA over several map segments as determined by the operator.

Propagation Map Construction, Export, and Analysis

Electrophysiological recordings before and after adenosine administration were processed for construction of propagation history maps. For each time period, a 5-second segment was taken, which in the case of adenosine corresponded with maximal atrioventricular conduction block. A 100 Hz low pass filter and 50 Hz notch filter were applied, outlier electrode signals were excluded after manual interrogation (to identify

spurious signals as a result of electrode damage during catheter insertion/preparation), and the QRS-T wave subtraction algorithm applied for all recordings (including those obtained after adenosine administration). Propagation maps were calculated and displayed using the default minimum amplitude sensitivity of 0.02 mV, time threshold of 70 ms (representing a conservative value for minimum atrial refractoriness) and window width of 80 ms (determining the duration of display of propagating wavefronts). Wavefront propagation patterns were evaluated using the AcQTrack system and data exported for analysis in custom designed software.

Propagation Pattern Quantification

For each 5-second map, AcQTrack data for LRA, LIA, and focal firing were extracted and quantified. Example patterns are shown in Figure 1 and a detailed explanation of the AcQTrack algorithm was outlined previously. A predefined method of pattern quantification was used in order to allow statistical comparison of activation patterns observed and is outlined in further detail in the Supplementary Methods and Figures S1

through S3. All occurrences for the segment were initially included and displayed as a static density map on the reconstructed anatomy. LRA and LIA were then quantified according to the raw number of occurrences of these patterns, the percentage of time over the segment that these patterns were present, and the percentage of atrial surface area covered. For focal firing, only the number of occurrences during the recording period were counted.

In order to correct for false positive pattern detection and isolated occurrences and to identify those regions in which specified activation patterns are repeatedly observed, a method of applying detection cutoffs was devised for LRA and LIA. A dynamic threshold, individualized for each recording is required given significant variation in frequency and duration of patterns across the chamber, which could result in a fixed frequency threshold, at a point suitable for 1 patient/map segment, either excluding all activation occurrences, or not sufficiently excluding regions with low relative frequency when applied to another recording. In addition, the relationship between frequency and duration of pattern occurrences is not fixed meaning that a

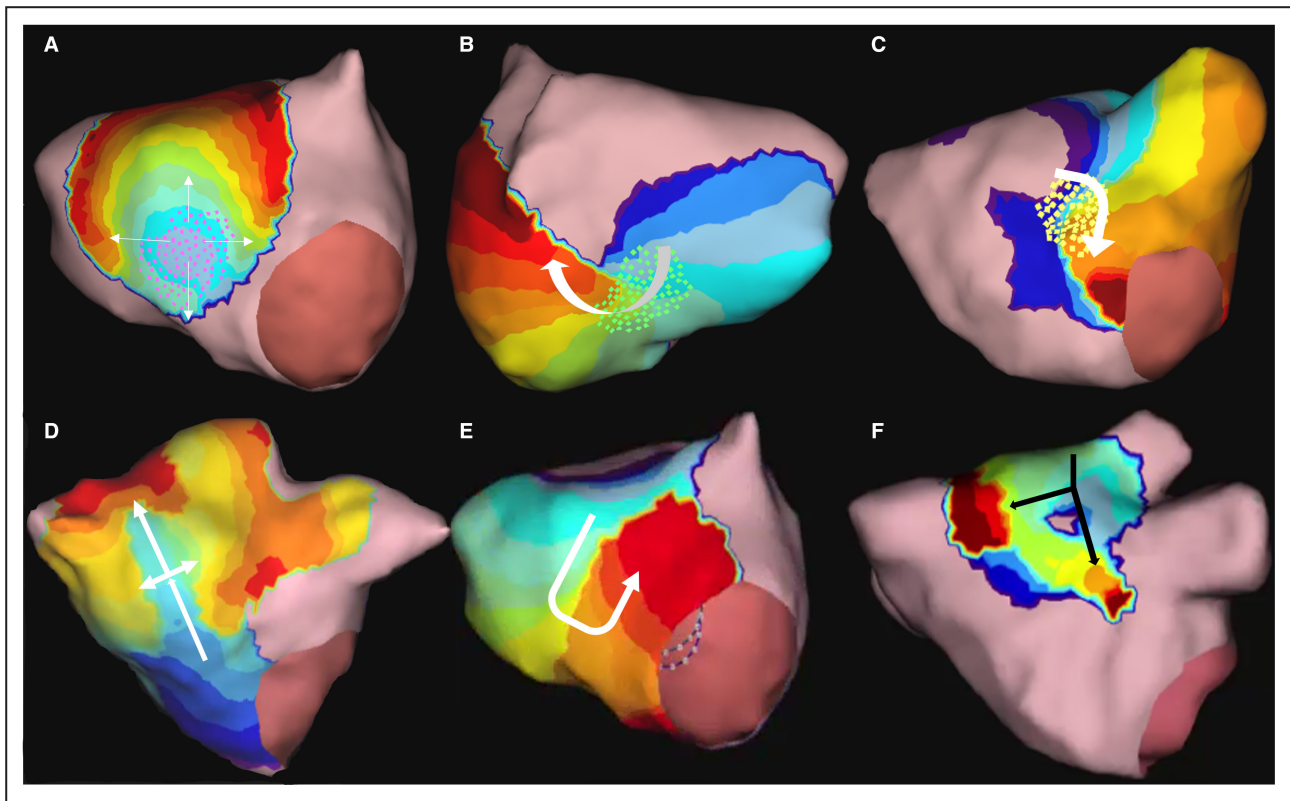


Figure 1. AcQTrack identifies FF (A) characterized by radial activation from a central earliest point, LRA (B) where smooth rotational activation of >270 degrees is observed; and LIA (C through F). LIA includes a range of specific patterns of activation, all characterized by changing wavefront direction of >90 degrees.

Pink, green, and yellow dots (A through C) are shown as examples of what can be seen during a procedure to illustrate the region in which FF, LRA, and LIA are detected using AcQTrack. FF indicates focal firing; LIA, localized irregular activation; and LRA, localized rotational activation.

threshold considering only a set percentage of pattern occurrences without including the duration these are present may be inadequate. First, a static map was generated with all pattern occurrences included and the percentage of time the pattern was present anywhere in the chamber was calculated. Occurrences were then excluded using cutoff values according to the frequency of each pattern that represent a 5%, 10%, 20%, 30%, and 40% relative drop in the total time the pattern was present resulting in gradually greater exclusion of regions with infrequent pattern occurrences and leaving those with the greatest frequency of detection (Figure 2). As well as measuring

the number of occurrences of each activation pattern, measuring the proportion of time these patterns are present over the fixed map duration (5 s) provides a measure of the duration that LIA or LRA persists and is therefore a marker of stability. Further detailed explanation is included in the supplementary methods.

Signal Processing and Dominant Frequency Analysis

Virtual electrograms from each vertex of the surface mesh (~3500 in total) making up the reconstructed anatomy were also exported for analysis and calculation of

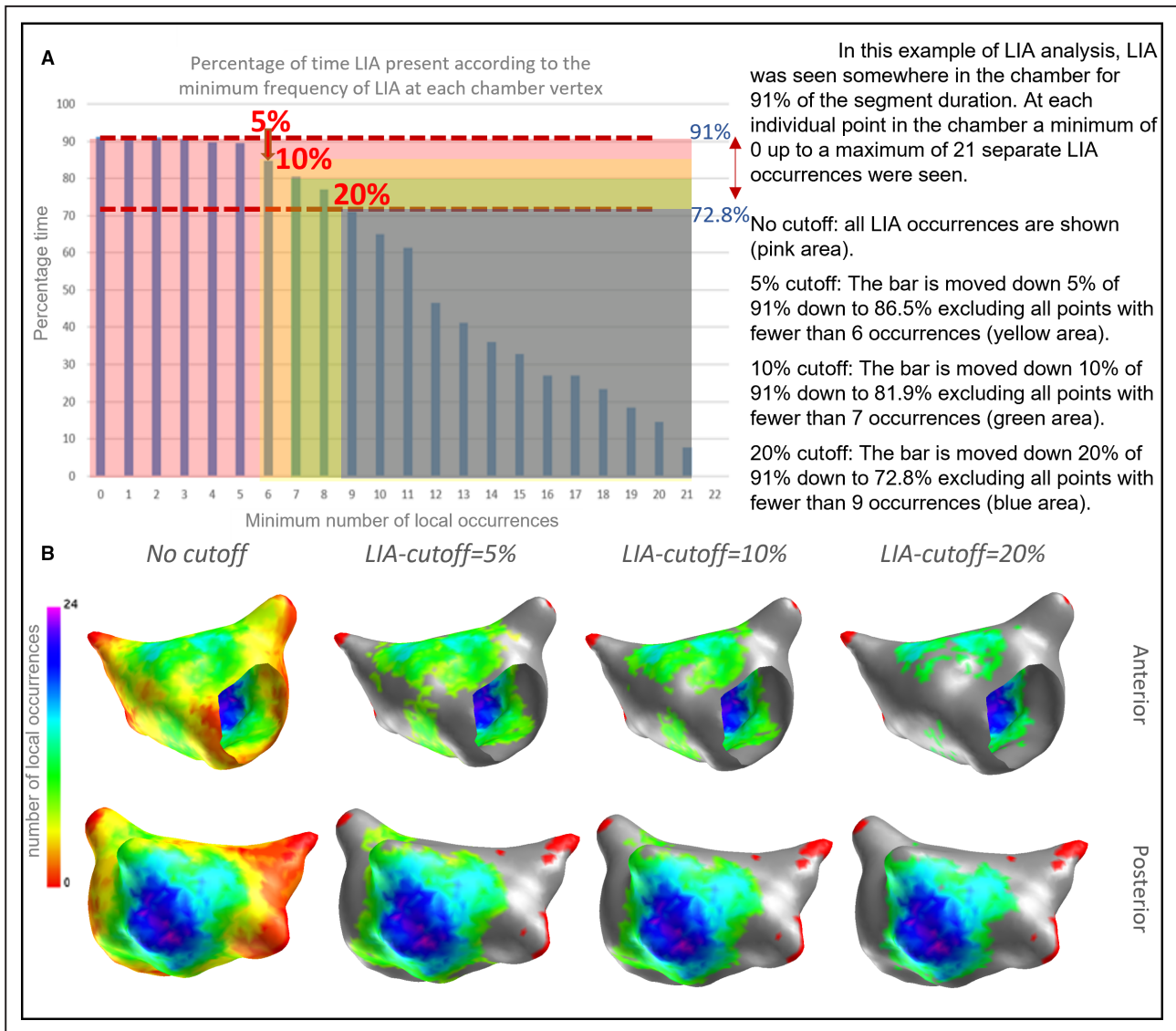


Figure 2. Method of applying cutoffs to LIA detection to exclude infrequent pattern occurrences
(A) With no cutoff applied, all occurrences are counted and the percentage of time occupied calculated (y axis). Cutoffs are then applied based on this analysis. Applying a 5%, 10%, and 20% relative reduction in the total time that patterns are present results in gradual exclusion of the least frequent occurrences below the minimum number of local occurrences (at each vertex) shown on the x axis. **(B)** In this example the 5% cutoff results in excluding regions with fewer than 6 LIA occurrences, with increasing exclusion with higher cutoffs. (Regions with excluded occurrences are shown in grey, red shows areas with no occurrences irrespective of cutoff). LIA indicates localized irregular activation.

atrial fibrillation cycle length (AFCL) and identification of phase singularities. Virtual electrograms were filtered and phase reconstruction achieved using a method of sinusoidal recomposition and the Hilbert transform as previously described.¹⁴ Phase singularity detection and lifespan calculation were then completed in line with previously described methods.¹⁵ For AFCL calculation, the cycle length at each nodal point was calculated for the 5 s recording from the phase signals and results for all signals combined to provide the mean global AFCL over the duration of the 5 s segment.

Virtual dipole signals were exported from each vertex of the chamber and dominant frequency (DF) identified as the maximum peak of the frequency-power spectrum at values within a presumed physiological range between 4 and 10 Hz after Fast Fourier Transform performed in Matlab (Mathworks 2019a). The mean and SD for all signals across the chamber were calculated to give the chamber DF value for comparison. Regions of high DF, defined as a localized zone with DF higher than all surrounding regions, were identified and compared with regions of high-frequency LRA.

Clinical Outcomes

Clinical outcomes were assessed according to acute procedural effects resulting in ablation terminating AF (either directly, or via an organized atrial tachycardia) or requiring direct current cardioversion to restore sinus rhythm. Differences in propagation patterns before and after adenosine were compared on the first map obtained in each patient (ie, at the earliest stage of the procedure) according to acute procedural outcome.

Statistical Analysis

Statistical analysis was performed using SPSS (version 25, IBM) or MatLab (Mathworks, R2019a). Continuous variables were assessed for normality of distribution using the Shapiro-Wilk test and expressed as mean±SD. Data were compared using the paired samples *t*-test comparing each map obtained with and without adenosine. Where differences were not normally distributed data were additionally transformed and analyzed using a 1-sample *t* test. If the results are concordant then the paired sample *t* test is reported. Categorical data are expressed as a number and percentage.

RESULTS

Patients

Twenty-two patients with persistent AF were included in the analysis. Mean age of the population was 60±12 and 68% were male. Other characteristics are shown in [Table 1](#). Maps with and without adenosine were

Table 1. Patient Characteristics for All Patients (n=22)

Characteristic	All patients
Age, y, mean (SD)	60±12
Male, n (%)	15 (68)
Body mass index, kg/m ² , median (Q1, Q3)	29 (25–30)
Amiodarone periprocedure, n (%)	6 (27)
Ejection fraction, %, median (Q1, Q3)	55 (54–60)
Left atrial diameter, mm, median (Q1, Q3)	45 (39–50)
Time since diagnosis, y, median (Q1, Q3)	3.5 (2–5)
First time procedure, n (%)	8 (47)
In atrial fibrillation at procedure start, n (%)	14 (82)

created before PVI in 11 participants, immediately after PVI in 15 participants, and after additional left atrial ablation in 9 participants resulting in a total of 35 paired maps. In all cases, a clear effect of adenosine on atrioventricular conduction was observed with a mean longest RR interval of 5708±2933 ms.

Wavefront Propagation Patterns

At baseline, the number of LIA occurrences was 99±20 (within the 5 s of recorded segment), which increased to 109±26 with adenosine, a statistically significant difference of 10 (95% CI, 2–19, *P*=0.012). When a 5% cutoff was used, LIA occurrences with adenosine were 83±16 compared with 76±15, reflecting a statistically significant difference of 7 (95% CI, 2.5–11, *P*=0.003). At 10%, 20%, 30%, and 40% cutoffs there was no difference in the number of LIA occurrences with adenosine (71±13 from 67±11, difference 4, 95% CI, –1.1 to 7.7, *P*=0.133; 53±9 from 51±9, difference 2, 95% CI, –1.8 to 4.7, *P*=0.372; 41±8 from 41±7, difference 0, 95% CI, –2.8 to 3.1, *P*=0.906; and 32±5 from 32±5, difference 0, 95% CI, –2.8 to 2.3, *P*=0.840 for 20%, 30%, and 40% cutoffs respectively—see [Table 2](#)). When analyzed as a percentage of time over which LIA occurred, adenosine resulted in a small but statistically significant increase in time LIA was present at all but the 40% cutoffs. The percentage of left atrial surface area in which LIA occurred was not affected by adenosine except for a small decrease in the surface area at the 30% (19.2±5.6 to 16.4±3.5, difference 2.8, 95% CI, 0.5–5, *P*=0.019) and 40% (14.0±5.4 to 11.6±3.0, difference 2.4, 95% CI, 0.4–4.3, *P*=0.021) cutoffs.

Irrespective of cutoff value, there was a significant increase in LRA with adenosine. The smallest increase in LRA occurrences was from 8.4±5.2 to 14.1±5.7 observed at the 20% cutoff (5.7, 95% CI, 2.7–8.6, *P*<0.0005), with the largest effect from 16.1±7.6 to 24.2±8.1 detected with no cutoff applied (8.1, 95% CI, 4.1–12, *P*<0.0005). The same pattern was observed when measured as a percentage of time LRA was

Table 2. Effect of Adenosine of LIA, LRA, and FF for All Maps, n=35 of 5-S Duration

Cutoff	Baseline (SD)	Adenosine (SD)	Difference (95% CI)	P value
LIA number of occurrences				
0%	99±20	109±26	10.0 (2 to 19)	0.012
5%	83±16	76±15	7 (2.5 to 11.0)	0.003
10%	67±11	71±13	3.3 (-1.1 to 7.7)	0.133
20%	51±9	53±9	1.5 (-1.8 to 4.7)	0.372
30%	41±7	41±8	0.2 (-2.8 to 3.1)	0.906
40%	32±5	32±5	-0.3 (-2.8 to 2.3)	0.840
LIA % time				
0%	76.4±11.1	79.9±12.4	3.5 (0.5 to 6.7)	0.025
5%	69.9±12.6	74.2±12.3	4.3 (1.5 to 7.2)	0.004
10%	66.2±11.2	70.2±11.0	4.0 (1.1 to 6.8)	0.007
20%	57.7±10.2	61.1±9.1	3.4 (1.0 to 5.8)	0.007
30%	50.1±8.2	52.9±9.6	2.7 (0.2 to 5.3)	0.035
40%	41.6±7.4	44.0±7.4	2.4 (-0.2 to 5.1)	0.072
LIA % surface area				
0%	85.8±11.3	86.1±13.8	0.3 (-3.5 to 4.0)	0.889
5%	46.1±10.0	46.4±10.2	0.3 (-3.6 to 4.2)	0.887
10%	37.9±7.8	35.6±8.4	-2.3 (-6.3 to 1.6)	0.242
20%	25.5±5.2	23.5±5.9	-2.0 (-4.5 to 0.4)	0.096
30%	19.2±5.6	16.4±3.5	-2.8 (-5.0 to -0.5)	0.019
40%	14.0±5.4	11.6±3.0	-2.4 (-4.3 to -0.4)	0.021
LRA number of occurrences				
0%	16.1±7.6	24.2±9.8	8.1 (4.1 to 12)	<0.0005
5%	11.3±6.5	18.6±8.1	7.3 (3.7 to 10.7)	<0.0005
10%	10.7±6.3	17.9±7.9	7.2 (4.0 to 10.5)	<0.0005
20%	8.4±5.2	14.1±6.4	5.7 (2.7 to 8.6)	<0.0005
30%	6.8±4.1	11.6±4.9	4.8 (2.6 to 6.7)	<0.0005
40%	5.5±3.3	10.2±4.3	4.7 (2.8 to 6.5)	<0.0005
LRA % time				
0%	29.8±11.8	43.3±15.5	13.5 (7.1 to 19.9)	<0.0005
5%	24.5±11.6	37.4±14.5	12.9 (6.8 to 19.0)	<0.0005
10%	23.6±36.3	36.3±14.1	12.7 (6.9 to 18.5)	<0.0005
20%	19.6±10.3	30.1±12.5	10.5 (4.9 to 16.3)	0.001
30%	17.0±9.0	25.5±10.3	8.5 (4.3 to 12.8)	<0.0005
40%	13.9±7.6	23.0±9.5	9.1 (5.0 to 13.1)	<0.0005
LRA % surface area				
0%	22.3±8.3	29.6±10.2	7.3 (3.3 to 11.3)	0.001
5%	12.7±6.5	16.0±6.7	3.3 (0.19 to 6.5)	0.038
10%	11.1±5.4	14.8±6.3	3.7 (1.1 to 6.2)	0.007
20%	7.7±3.3	10.1±4.1	2.4 (0.6 to 4.2)	0.012
30%	6.0±2.5	7.7±3.7	1.7 (0.6 to 3.0)	0.005
40%	4.7±2.2	6.3±2.8	1.6 (0.6 to 2.7)	0.004
FF numbers				
	24.5±8.2	22.0±7.33	-2.5 (-6 to 1.2)	0.18

FF indicates focal firing; LIA, localized irregular activation; and LRA, localized rotational activation.

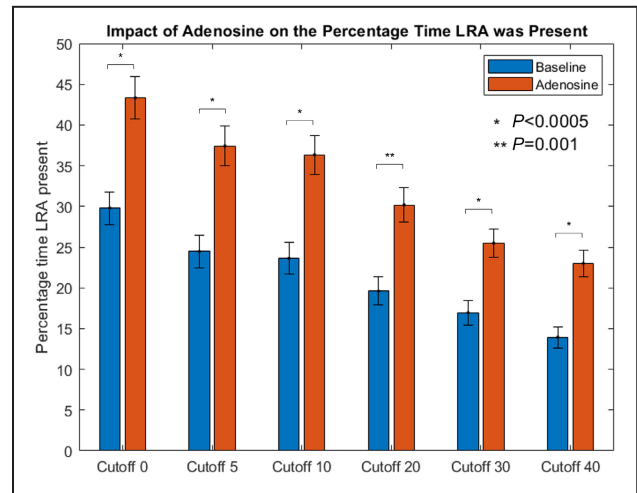


Figure 3. Effect of adenosine on percentage time of LRA occurrences for all maps (n=35).

LRA indicates localized rotational activation. Bars represent SE.

present as illustrated in Figure 3. Adenosine administration resulted in a small increase in the proportion of the left atrium surface area in which LRA occurred. See Table 2 for full results. Examples of the effect of adenosine are shown in Videos S1 and S2 and in Figure 4.

Although differences were observed at all stages, this did not reach statistical significance at baseline, and was most pronounced post PVI and after nonpulmonary vein ablation (see Figure 5 and Table S1).

Adenosine had no significant effect on the number of focal firings observed (24.5±8.2 versus 22.0±7.3 at baseline, difference -2.5, 95% CI, -6 to 1.2, P=0.18).

AF Cycle Length

At baseline, AFCL was 181.7±14.3 ms, which reduced to 165.1±16.3 ms with adenosine, a mean shortening of 16.6 ms (95% CI, 11.3–21.9, P<0.0005). The value for the fifth percentile of AFCL in each map was also analyzed to reflect the fastest activation rates, proposed as a surrogate of refractoriness. Adenosine resulted in a similar shortening of the fifth percentile of AFCL from 135.0±11.1 ms to 127.5±12.2 ms, a mean reduction of 7.5 ms (95% CI, 3.8–11.2, P<0.0005). The coefficient of variance of AFCL (SD/mean) was 0.072±0.028 at baseline, and 0.052±0.016 with adenosine (difference 0.020, 95% CI, 0.01–0.03, P<0.0005).

There was a concomitant increase in global DF with adenosine from a mean of 6.0±0.7 Hz to 6.6±0.8 Hz, a statistically significant mean difference of 0.6Hz (95% CI, 0.4–0.9, P<0.0005). Coefficient of variance in DF reduced with adenosine from 0.08±0.05 to 0.06±0.02, but this was not statistically significant (mean difference 0.02, 95% CI, -0.003 to 0.03, P=0.0915).

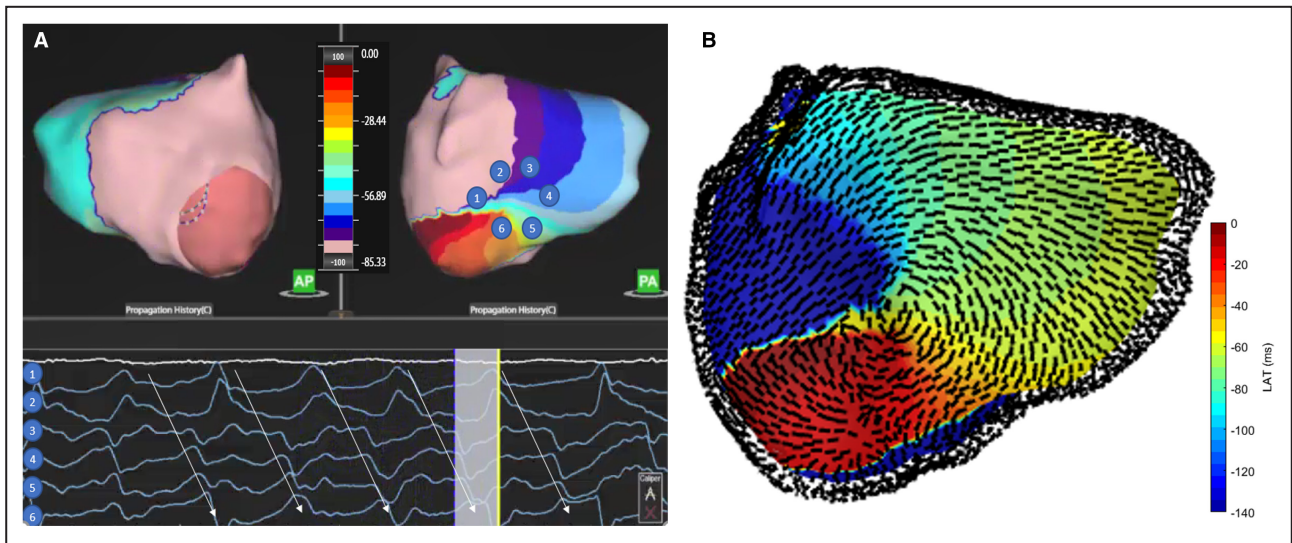


Figure 4. Example activation map of a zone of LRA on the inferoposterior LA seen after adenosine injection (A). Dipole signals around this rotational pivot point demonstrate progressive activation. The same pattern of activation is shown in Videos S1 and S2 and the conduction velocity vector map (B) demonstrates the angles of propagation around the central point. AP indicates anterior posterior; LA, left atrium; LRA, localized rotational activation; and PA, posterior anterior.

Phase Singularities

Multiple short-lasting phase singularities were found in all recordings. There were a greater number of phase singularities seen with adenosine (36.6 ± 9.3) compared with baseline (30.1 ± 7.8), which represented a statistically significant mean difference of 6.5 (95% CI, 2.6–10.0, $P=0.002$). There was a small but statistically significant increase in the lifespan of phase singularities with adenosine from 509 ± 161 to 599 ± 245 ms (90; 95% CI, 13–167; $P=0.023$).

Spatial distribution of LRA

In light of the observation of LRA occurring over a greater left atrium surface area with adenosine, each map was visually inspected at the highest cutoff to identify whether regions with repetitive LRA remained spatially consistent or were changed with adenosine use. At baseline, a region of repetitive LRA could be identified in 89% (31 of the 35) of maps, with 61 zones identified in total (1.7 ± 1.1 per map). Following adenosine infusion, 70 zones were identified across all 35 maps (2 ± 1 per map), with 42 of these zones (60%; 1.2 ± 1.0 per map) localized to the same site as LRA in baseline maps. Figure 6 illustrates regions of repetitive LRA in 2 patients before and after adenosine infusion. Regions of high-frequency LIA and LRA may overlap, given that multiple wavefronts over different AF cycles may or may not satisfy criteria for LRA within the same confined region (eg, partial rotation through 180 degrees) and be classified as LIA. A total of 81% of sites with high-frequency LRA with adenosine coincided with sites where high-frequency LIA was seen on baseline maps. There were 11 maps (in 9 patients) where the zones of LRA observed in adenosine maps were all in different sites from the baseline maps. In 4 of these, there were no regions of repetitive LRA seen at baseline.

In those patients where mapping was performed at more than 1 time point during the procedure ($n=12$; 1 patient had maps at all 3 time points), regions with the highest frequency of LRA seen on adenosine maps were compared. Across maps, 54 sites were identified, with 15 (28%) of these present at more than 1 time point during the procedure.

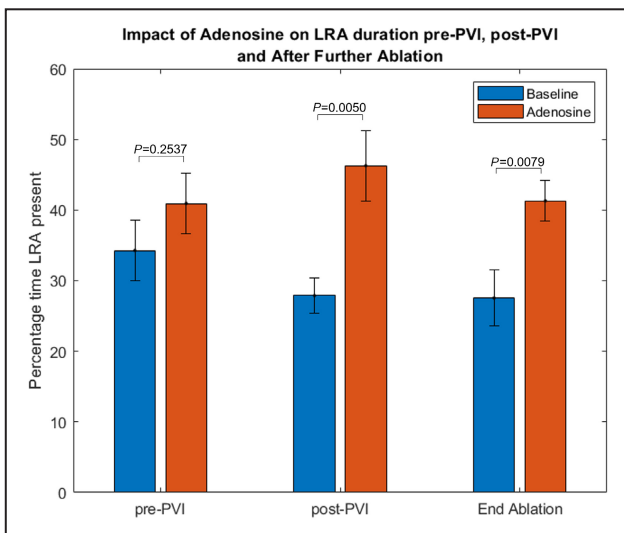


Figure 5. Effect of adenosine on LRA duration before and after pulmonary vein isolation, and after nonpulmonary vein ablation (bars represent standard error). ($n=11$ pre-PVI, $n=15$ post-PVI, $n=9$ end ablation). LRA indicates localized rotational activation; and PVI, pulmonary vein isolation.

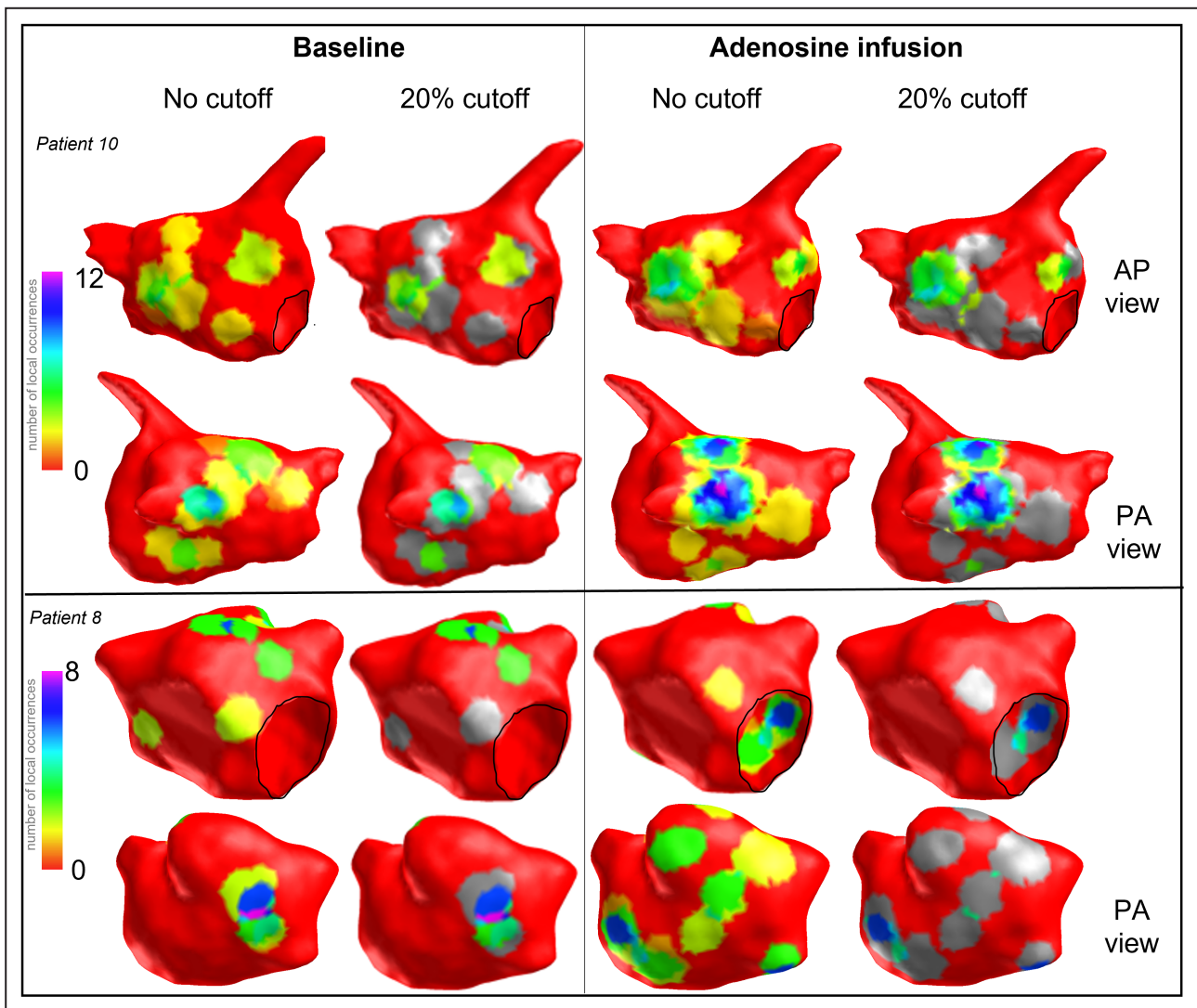


Figure 6. Regions of highly repetitive LRA after adenosine infusion identified at 20% cutoff threshold (in pink/purple) occur at regions of LRA at baseline at lower frequency in patient 10 (top images) in contrast with patient 8 (lower panel) in whom adenosine promotes LRA in regions widely distributed throughout the chamber with little correlation to those zones seen at baseline.

Mitral annulus is outlined in black, areas of excluded occurrences are shown in grey. AP indicates anterior posterior; LRA, localized rotational activation; and PA, posterior anterior.

Across 26 maps at baseline, 40 sites of high DF were identified with 13 of these (33%) correlating with sites of high-frequency LRA. After adenosine injection, 44 high DF sites were identified (in 30 maps), with 12 (27%) of these aligning with sites of high-frequency LRA (see Figure 7).

Clinical Outcomes

Ablation resulted in acute termination to sinus rhythm in 6 (27%), with the remainder undergoing direct current cardioversion at the end of the procedure. Those in whom direct current cardioversion was required had more LRA on baseline maps compared with patients in whom ablation terminated AF. This was most

prominent at 20% cutoff when measured as a number of LRA occurrences (9.0 ± 5.2 versus 3.7 ± 2.3 , 95% CI, 0.7–10, $P=0.0270$), proportion of time LRA was present (20.8 ± 10.8 versus 10.3 ± 6.5 , 95% CI, 0.6–20.5, $P=0.0380$) or the surface area affected (8.3 ± 3.3 versus 3.9 ± 2.3 , 95% CI, 1.3–7.5, $P=0.0080$). There was no difference between the 2 groups on adenosine maps on any measure. See Tables S2 and S3 for full results.

DISCUSSION

The main findings of our study are that intravenous adenosine injection has the following effects on AF: (1) AFCL shortening with increase in DF, (2) a modest

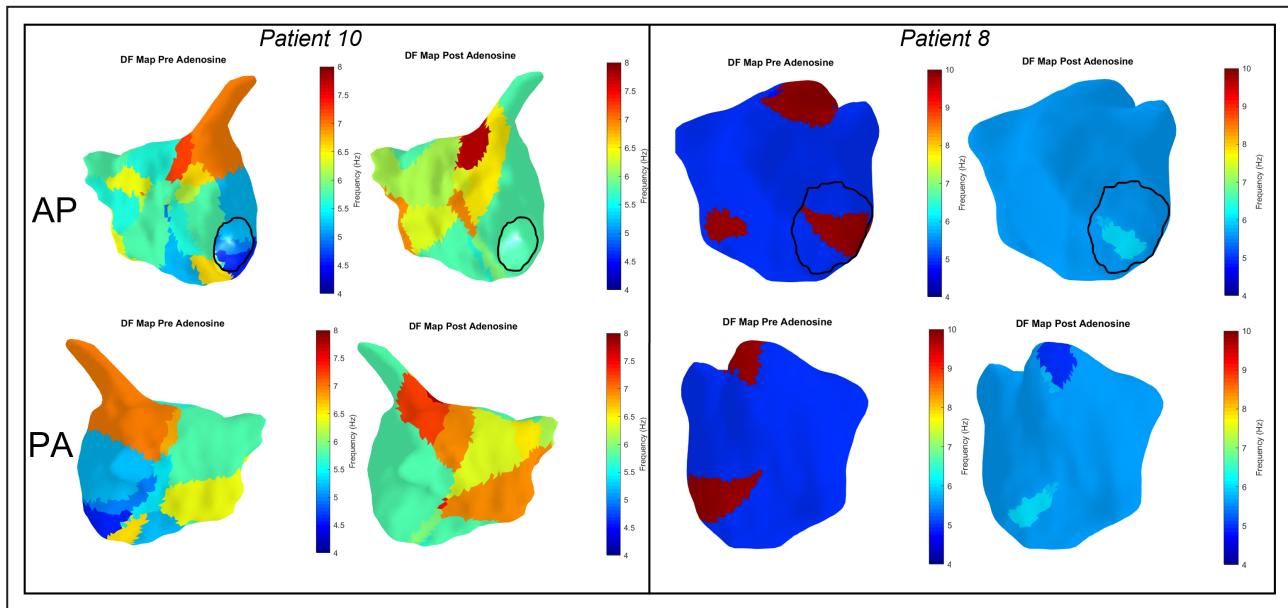


Figure 7. Dominant frequency (DF) maps for the same patients included in Figure 6.

A zone of highest DF in patient 10 is seen at the base of the LAA in the AP view both before and after adenosine injection, which does not correlate with the region of high-frequency LRA seen on the posterior wall (see Figure 6). Zones of high DF are also seen in patient 8 in the septum, roof, and mitral isthmus at baseline. A region of high-frequency LRA is seen on the roof of the LA (Figure 6) but there is no correlation with other zones of high DF. A region of high DF in the posterolateral mitral isthmus after adenosine correlates with a site of LRA. Mitral annulus is outlined in black, color scale ranges from lowest to highest DF in each patient. AP indicates anterior posterior; LA, left atrium; LRA, localized rotational activation; and PA, posterior anterior.

increase in wave propagation irregularity (as defined by LIA parameter), (3) marked increase in the number of short-lasting rotating waves (assessed both by activation time and phase singularity mapping), and (4) an increase in the lifespan of rotating waves. We found no effect of adenosine on focal firing frequency. Although the majority (60%) of regions found to have high LRA counts on adenosine maps were consistent with the zones identified at baseline, 40% of regions seen were revealed only with use of adenosine and only 28% were consistent across multiple mapping time points.

The mechanisms responsible for maintenance of persistent AF are poorly understood. Early studies in animal models led to the description of localized rotors, defined as organized and repetitive reentry circuits thought to represent organized drivers.^{16–19} In recent years, efforts have focused on developing techniques to map these sources to guide additional ablation beyond the pulmonary veins in a bid to improve clinical outcomes. Although early results of this strategy were promising,^{20–23} recent randomized studies evaluating this approach have been disappointing.²⁴ Furthermore, these methods have primarily relied on a phase mapping approach applied either to multielectrode basket catheters or noninvasive body surface electrodes, which aim to identify phase singularities representing the pivot point of localized rotors.²⁵ Further studies and evaluation of this technique have revealed

contrasting results and highlighted the limitations of this approach.^{26–29}

The noncontact mapping employed in this study reveals patterns of propagation based on charge density reconstruction.¹² Uniquely, this system allows visualization of the dynamics of wavefront propagation during AF and reveals recurrent patterns of partial rotation, directional changes, conduction slowing, and focal firing with a high degree of spatial stability.¹² Although the ionic effects of adenosine have been well defined, the functional impact of these changes on wavefront propagation are less clear. The presumption that hyperpolarizing the atrial myocardial cell membrane, as well as shortening action potential duration and refractoriness, promotes reentry appears theoretically sound and is supported by our results with the predominant effect of adenosine being a promotion of LRA.³⁰ Hansen et al showed that adenosine promoted local reentry at sites of AF termination or cycle length slowing, proposed as evidence of adenosine unmasking sites of reentry driving AF propagation.¹⁰ However, although 9 of the 15 sites identified (in the 10 patients studied) were more pronounced with adenosine, 6 were not.¹⁰ We found that only 28% of sites identified with adenosine were stable between recordings. Moreover, the rotational activation promoted by adenosine was evident both in regions with repetitive patterns (as identified using the higher cutoffs) but also distributed more widely through

the chamber (seen with no cutoff applied). Patients in whom ablation terminated AF had less rotational activation at baseline but the effect of adenosine was the same irrespective of acute procedural outcome, which is not in keeping with the theory that sites revealed with the use of adenosine represent arrhythmogenic sources responsible for AF propagation. The degree of rotational activation measured after adenosine appears to represent the pharmacological properties of the drug, independent of the individual substrate properties of the patient. The degree of rotational activation before adenosine administration was, however, lower in patients in whom ablation achieved sinus rhythm. It may be that the degree of rotational activation seen serves as a surrogate marker of atrial functional electrophysiological properties that affect the likelihood of acute termination, but these are concealed by use of adenosine rather than revealed and do not provide evidence that targeting ablation to areas identified with the use of adenosine are likely to yield improved procedural outcomes.

Sites of high-frequency LRA and LIA may overlap as these both represent localized directional changes in propagation. A total of 81% of LRA zones identified using adenosine occurred in regions with high-frequency LIA at baseline. Reentry mechanisms have been shown to anchor to structural heterogeneities,^{31,32} whereas LIA zones are highly stable between recordings, perhaps reflective of local structural abnormalities or anatomical complexities,³³ which results in directional change in propagation at these sites. Shortening of atrial refractoriness with adenosine enables the directional change to complete >270 degrees of rotation and persist for longer therefore appearing as LRA. Importantly, these are generally short-lived patterns of incomplete rotation rather than stable complete reentry. Zaman et al reviewed reconstructed isochronal maps from sites of acute AF termination during ablation of persistent AF guided by focal impulse and rotor modulation mapping. The predominant activation pattern seen was that of incomplete rotation (in 46%) with stable rotational sources identified in only 21%, in keeping with high-density contact mapping studies.^{34,35} We did not find stable rotating waves using both approaches (LRA and phase singularity mapping). It may be that regions of high-frequency LIA best reflect anatomical properties that affect wavefront propagation, with LRA determined by functional atrial properties. Importantly, the patterns of LRA promoted by adenosine occur in a spatiotemporally diverse distribution and are therefore of limited clinical relevance when devising ablation strategies.

No effect on focal firing was observed. Hyperpolarization of the atrial myocardial cell membrane results in slowing in the rate of diastolic depolarization thus reducing automaticity. In addition,

adenosine is known to inhibit catecholaminergic sensitive L-type inward calcium currents within the atria.³⁰ Importantly, however, all the patients included in our analysis had persistent AF. Adenosine appears to have differential effects in patients with paroxysmal versus persistent arrhythmia possibly because of the relative difference in etiological contribution of the pulmonary veins and wider atrial myocardial substrate.^{5,6} Increased pulmonary vein firing after adenosine infusion is well described but is likely to be of greater significance in paroxysmal AF and not observed during persistent arrhythmia.^{36,37} Furthermore, apparent focal firing during persistent AF may be related to epicardial to endocardial breakthrough rather than automaticity (which is not affected by adenosine).³⁸ Reentry mechanisms may occur at the micro-anatomic level, detectable only using high-resolution optical mapping³² and not revealed at the resolution of the clinical mapping system used in this study. However, if present and promoted by adenosine, then it would be anticipated that this would manifest as an increase in focal activations appearing on the endocardial surface, which was not observed.

These results suggest a global acceleration of AF within the left atrium as demonstrated by a reduction in mean AFCL with significant (albeit small) reduction in variation of AFCL from 7.2% to 5.2% (measured by coefficient of variance of AFCL), which is supported by the concomitant increase in DF. This suggests a global atrial pharmacological effect rather than limited focal changes that would be expected to cause greater heterogeneity in AFCL (or DF) across the chamber.

Limitations

These results are restricted to analysis of left atrial propagation. The distribution of adenosine receptors is heterogeneous⁷ and in persistent AF, an increase in dominant frequency with adenosine was demonstrated only in the high right atrium.⁶ The right atrium is known to represent sites of mechanistic significance in a proportion of patients with AF and a differential effect of adenosine on right atrial propagation cannot be excluded.^{21,39}

Only short segments of maps (5 s duration) were analyzed. Spatiotemporal variation in AF propagation may mean that patterns of propagation change during different or longer map durations. The differences observed after adenosine administration were highly consistent suggesting this was not simply the result of a different time period of measurement. Although an increase in LIA was also observed, these changes were small, only significant (in terms of number of pattern occurrences) in raw analysis and 5% cutoff, and not likely to be clinically significant. Given the whole chamber acceleration in AFCL, a greater number of

AF cycles would be expected over the same recording period and a small increase in the occurrences of infrequent spatially diverse irregular activation may therefore be observed. Furthermore, the proportion of time LIA patterns were present increased by only 3.2%–3.8%, which is unlikely to be significant and may also be driven by the reduction in refractoriness.

The technology used in this study is based on the resolution of local charge density derived through application of the inverse solution to multiple simultaneously recorded intracavitary unipolar electrograms.¹² Electrical activity on the endocardial surface (discretized as ≈ 3500 vertices) is obtained as an inverse solution based on measurements of 48 electrodes of the basket catheter. This is a unique approach aimed at achieving a more accurate local representation of cardiac activation and has been validated against contact unipolar recordings.⁴⁰ However, the precise implication of this technique on the visualized map of atrial activation compared with alternative techniques is difficult to discern and requires further extensive comparison given the lack of sufficient validation of activation patterns against contact recordings or optical mapping during AF.

It is difficult to establish the effect of ablation. The effects on LRA were consistent at all stages of the procedure but not statistically significant before any ablation. The primary analysis was intended to detect an effect across all maps and may have been underpowered to detect differences with subanalyses. The difference in statistical significance was driven in part by a reduction in LRA observed post PVI, which may be the result of pulmonary vein ablation incorporating sites of LRA. However, this difference was not statistically significant and if PVI eliminated rotational sites it would be anticipated that this would also reduce the impact of adenosine, which was not observed. Although the number of rotational activation patterns were lower in patients in whom ablation was acutely successful, it is difficult to draw further conclusions about the process of sinus rhythm restoration, which was not seen to occur instantaneously after ablation delivery. It cannot therefore be determined whether the first area targeted, or the last, or a combination of all of them was the critical mechanism maintaining AF. Furthermore, although we report acute procedural outcomes, these may not correspond to clinically meaningful long-term outcomes, which would require further analyses beyond the scope of this study.

CONCLUSIONS

Our results suggest that rotational activation, in contrast with focal firing, and much less so LIA, is influenced by adenosine. Adenosine allows for a higher

density of rotating wavefronts at spatially variable sites throughout the left atrium and shorter global cycle length with increase in DF. The degree of rotational activation may serve as a surrogate measure of individual atrial functional properties, with little evidence that rotational activation seen with adenosine represents promising targets for ablation aimed at arrhythmogenic sources of AF perpetuation within the left atrium particularly as there is little stability of LRA sites within patients. Caution should be exercised when interpreting maps obtained after adenosine administration to guide nonpulmonary vein ablation.

ARTICLE INFORMATION

Received February 3, 2021; accepted March 18, 2022.

Affiliations

Oxford University Hospitals NHS Foundation Trust, Oxford, United Kingdom (M.T.P., A.B.e., M.L., T.R.B.); University of Southampton, United Kingdom (M.T.P., M.M., J.P.); Department of Cardiology, Asklepios Clinic St. Georg, Hamburg, Germany (P.K.); Southampton University Hospitals NHS Foundation Trust, Southampton, United Kingdom (M.M., J.P.); and University of Oxford Biomedical Research Centre, Oxford, United Kingdom (T.R.B.).

Sources of Funding

This study was supported by the Oxford Biomedical Research Centre and funded by internal departmental budgets.

Disclosures

Michael Pope has received honoraria and support for conference attendance from Acutus Medical. Pawel Kuklik provides consultancy services to Acutus Medical. Timothy Betts has received honoraria from Acutus Medical and is a member of the Medical Advisory Board.

Supplemental Material

Data S1
Tables S1–S3
Figures S1–S4
Videos S1–S2

REFERENCES

1. Belhassen B, Pelleg A, Shoshani D, Laniado S. Atrial fibrillation induced by adenosine triphosphate. *Am J Cardiol.* 1984;53:1405–1406. doi: [10.1016/0002-9149\(84\)90104-8](https://doi.org/10.1016/0002-9149(84)90104-8)
2. Nakai T, Watanabe I, Kunimoto S, Kojima T, Kondo K, Saito S, Ozawa Y, Kanmatsuse K. Electrophysiological effect of adenosine triphosphate and adenosine on atrial and ventricular action potential duration in humans. *Jpn Circ J.* 2000;64:430–435. doi: [10.1253/jcj.64.430](https://doi.org/10.1253/jcj.64.430)
3. Belardinelli L, Isenberg G. Isolated atrial myocytes: adenosine and acetylcholine increase potassium conductance. *Am J Physiol.* 1983;244:H734–H737. doi: [10.1152/ajpheart.1983.244.5.H734](https://doi.org/10.1152/ajpheart.1983.244.5.H734)
4. Drury AN, Szent-Györgyi A. The physiological activity of adenine compounds with especial reference to their action upon the mammalian heart. *J Physiol.* 1929;68:213–237.
5. Berenfeld O. Ionic and substrate mechanism of atrial fibrillation: rotors and the exitation frequency approach. *Arch Cardiol Mex.* 2010;80:301–314.
6. Atienza F, Almendral J, Moreno J, Vaidyanathan R, Talkachou A, Kalifa J, Arenal A, Villacastín JP, Torrecilla EG, Sánchez A, et al. Activation of inward rectifier potassium channels accelerates atrial fibrillation in humans: evidence for a reentrant mechanism. *Circulation.* 2006;114:2434–2442. doi: [10.1161/CIRCULATIONAHA.106.633735](https://doi.org/10.1161/CIRCULATIONAHA.106.633735)
7. Li N, Csepe TA, Hansen BJ, Sul LV, Kalyanasundaram A, Zakharkin SO, Zhao J, Guha A, Van Wagoner DR, Kilic A, et al. Adenosine-induced atrial fibrillation: localized reentrant drivers in lateral right atria due to

- heterogeneous expression of adenosine A1 Receptors and GIRK4 subunits in the human heart. *Circulation*. 2016;134:486–498. doi: [10.1161/CIRCULATIONAHA.115.021165](https://doi.org/10.1161/CIRCULATIONAHA.115.021165)
8. Sarmast F, Kolli A, Zaitsev A, Parisian K, Dharmoon AS, Guha PK, Warren M, Anumonwo JM, Taffet SM, Berenfeld O, et al. Cholinergic atrial fibrillation: I(K, ACh) gradients determine unequal left/right atrial frequencies and rotor dynamics. *Cardiovasc Res*. 2003;59:863–873. doi: [10.1016/S0008-6363\(03\)00540-6](https://doi.org/10.1016/S0008-6363(03)00540-6)
 9. Sanders P, Berenfeld O, Hocini M, Jais P, Vaidyanathan R, Hsu L-F, Garrigue S, Takahashi Y, Rotter M, Sacher F, et al. Spectral analysis identifies sites of high-frequency activity maintaining atrial fibrillation in humans. *Circulation*. 2005;112:789–797. doi: [10.1161/CIRCULATIONAHA.104.517011](https://doi.org/10.1161/CIRCULATIONAHA.104.517011)
 10. Hansen BJ, Zhao J, Helfrich KM, Li N, Lancau A, Zolotarev AM, Zakharkin SO, Kalyanasundaram A, Subr M, Dastagir N, et al. Unmasking arrhythmogenic hubs of reentry driving persistent atrial fibrillation for patient-specific treatment. *J Am Heart Assoc*. 2020;9:e017789. doi: [10.1161/JAHA.120.017789](https://doi.org/10.1161/JAHA.120.017789)
 11. Shi R, Norman M, Chen Z, Wong T. Individualized ablation strategy guided by live simultaneous global mapping to treat persistent atrial fibrillation. *Future Cardiol*. 2018;14:237–249. doi: [10.2217/fca-2017-0109](https://doi.org/10.2217/fca-2017-0109)
 12. Grace A, Willems S, Meyer C, Verma A, Heck P, Zhu M, Shi X, Chou D, Dang L, Scharf C, et al. High-resolution noncontact charge-density mapping of endocardial activation. *JCI Insight*. 2019;4. doi: [10.1172/jci.insight.126422](https://doi.org/10.1172/jci.insight.126422)
 13. Willems S, Verma A, Betts TR, Murray S, Neuzil P, Ince H, Steven D, Sultan A, Heck PM, Hall MC, et al. Targeting nonpulmonary vein sources in persistent atrial fibrillation identified by noncontact charge density mapping. *Circ Arrhythm Electrophysiol*. 2019;12:e007233. doi: [10.1161/CIRCEP.119.007233](https://doi.org/10.1161/CIRCEP.119.007233)
 14. Kuklik P, Zeemering S, Maesen B, Maessen J, Crijns HJ, Verheule S, Ganesan AN, Schotten U. Reconstruction of instantaneous phase of unipolar atrial contact electrogram using a concept of sinusoidal recomposition and Hilbert transform. *IEEE Trans Biomed Eng*. 2015;62:296–302. doi: [10.1109/TBME.2014.2350029](https://doi.org/10.1109/TBME.2014.2350029)
 15. Kuklik P, Zeemering S, van Hunnik A, Maesen B, Pison L, Lau DH, Maessen J, Podziemski P, Meyer C, Schaffer B, et al. Identification of rotors during human atrial fibrillation using contact mapping and phase singularity detection: technical considerations. *IEEE Trans Biomed Eng*. 2017;64:310–318.
 16. Mandapati R, Skanes A, Chen J, Berenfeld O, Jalife J. Stable microentrant sources as a mechanism of atrial fibrillation in the isolated sheep heart. *Circulation*. 2000;101:194–199. doi: [10.1161/01.CIR.101.2.194](https://doi.org/10.1161/01.CIR.101.2.194)
 17. Jalife J, Berenfeld O, Skanes A, Mandapati R. Mechanisms of atrial fibrillation: mother rotors or multiple daughter wavelets, or both? *J Cardiovasc Electrophysiol*. 1998;9:S2–S12.
 18. Jalife J. Rotors and spiral waves in atrial fibrillation. *J Cardiovasc Electrophysiol*. 2003;14:776–780. doi: [10.1046/j.1540-8167.2003.03136.x](https://doi.org/10.1046/j.1540-8167.2003.03136.x)
 19. Jalife J, Berenfeld O, Mansour M. Mother rotors and fibrillatory conduction: a mechanism of atrial fibrillation. *Cardiovasc Res*. 2002;54:204–216. doi: [10.1016/S0008-6363\(02\)00223-7](https://doi.org/10.1016/S0008-6363(02)00223-7)
 20. Narayan SM, Krummen DE, Shivkumar K, Clopton P, Rappel WJ, Miller JM. Treatment of atrial fibrillation by the ablation of localized sources: CONFIRM (Conventional Ablation for Atrial Fibrillation With or Without Focal Impulse and Rotor Modulation) trial. *J Am Coll Cardiol*. 2012;60:628–636. doi: [10.1016/j.jacc.2012.05.022](https://doi.org/10.1016/j.jacc.2012.05.022)
 21. Miller JM, Kalra V, Das MK, Jain R, Garlie JB, Brewster JA, Dandamudi G. Clinical benefit of ablating localized sources for human atrial fibrillation: the Indiana University FIRM Registry. *J Am Coll Cardiol*. 2017;69:1247–1256. doi: [10.1016/j.jacc.2016.11.079](https://doi.org/10.1016/j.jacc.2016.11.079)
 22. Miller JM, Kowal RC, Swarup V, Daubert JP, Daoud EG, Day JD, Ellenbogen KA, Hummel JD, Baykaner T, Krummen DE, et al. Initial independent outcomes from focal impulse and rotor modulation ablation for atrial fibrillation: multicenter FIRM registry. *J Cardiovasc Electrophysiol*. 2014;25:921–929. doi: [10.1111/jce.12474](https://doi.org/10.1111/jce.12474)
 23. Haissaguerre M, Hocini M, Denis A, Shah AJ, Komatsu Y, Yamashita S, Daly M, Amraoui S, Zellerhoff S, Picat M-Q, et al. Driver domains in persistent atrial fibrillation. *Circulation*. 2014;130:530–538. doi: [10.1161/CIRCULATIONAHA.113.005421](https://doi.org/10.1161/CIRCULATIONAHA.113.005421)
 24. Brachmann JHJ, Wilber DJ, Sarver AE, Rapkin J, Shpun S, Szili-Torok T. Prospective randomized comparison of rotor ablation vs conventional ablation for treatment of persistent atrial fibrillation - The REAFFIRM trial. *Heart Rhythm*. 2019;16:963.
 25. Umapathy K, Nair K, Masse S, Krishnan S, Rogers J, Nash MP, Nanthakumar K. Phase mapping of cardiac fibrillation. *Circ Arrhythm Electrophysiol*. 2010;3:105–114. doi: [10.1161/CIRCEP.110.853804](https://doi.org/10.1161/CIRCEP.110.853804)
 26. Child N, Clayton RH, Roney CR, Laughner JJ, Shuros A, Neuzil P, Petru J, Jackson T, Porter B, Bostock J, et al. Unraveling the underlying arrhythmia mechanism in persistent atrial fibrillation: results from the STARLIGHT study. *Circ Arrhythm Electrophysiol*. 2018;11:e005897. doi: [10.1161/CIRCEP.117.005897](https://doi.org/10.1161/CIRCEP.117.005897)
 27. Laughner J, Shome S, Child N, Shuros A, Neuzil P, Gill J, Wright M. Practical considerations of mapping persistent atrial fibrillation with whole-chamber basket catheters. *JACC Clin Electrophysiol*. 2016;2:55–65. doi: [10.1016/j.jacep.2015.09.017](https://doi.org/10.1016/j.jacep.2015.09.017)
 28. Rodrigo M, Climent AM, Liberos A, Fernández-Avilés F, Berenfeld O, Atienza F, Guillem MS. Technical considerations on phase mapping for identification of atrial reentrant activity in direct- and inverse-computed electrograms. *Circ Arrhythm Electrophysiol*. 2017;10. doi: [10.1161/CIRCEP.117.005008](https://doi.org/10.1161/CIRCEP.117.005008)
 29. Roney CH, Cantwell CD, Bayer JD, Qureshi NA, Lim PB, Tweedy JH, Kanagaratham P, Peters NS, Vigmond EJ, Ng FS. Spatial resolution requirements for accurate identification of drivers of atrial fibrillation. *Circ Arrhythm Electrophysiol*. 2017;10:e004899. doi: [10.1161/CIRCEP.116.004899](https://doi.org/10.1161/CIRCEP.116.004899)
 30. Belardinelli L, Shryock JC, Song Y, Wang D, Srinivas M. Ionic basis of the electrophysiological actions of adenosine on cardiomyocytes. *FASEB J*. 1995;9:359–365. doi: [10.1096/fasebj.9.5.7896004](https://doi.org/10.1096/fasebj.9.5.7896004)
 31. Haissaguerre M, Shah AJ, Cochet H, Hocini M, Dubois R, Efimov I, Vigmond E, Bernus O, Trayanova N. Intermittent drivers anchoring to structural heterogeneities as a major pathophysiological mechanism of human persistent atrial fibrillation. *J Physiol*. 2016;594:2387–2398. doi: [10.1113/JP270617](https://doi.org/10.1113/JP270617)
 32. Hansen BJ, Zhao J, Csepe TA, Moore BT, Li N, Jayne LA, Kalyanasundaram A, Lim P, Bratasz A, Powell KA, et al. Atrial fibrillation driven by micro-anatomic intramural re-entry revealed by simultaneous sub-epicardial and sub-endocardial optical mapping in explanted human hearts. *Eur Heart J*. 2015;36:2390–2401. doi: [10.1093/eurheartj/ehv233](https://doi.org/10.1093/eurheartj/ehv233)
 33. Pope MT, Kuklik P, Briosca EGA, Leo M, Mahmoudi M, Paisey J, Betts TR. Spatial and temporal variability of rotational, focal, and irregular activity: practical implications for mapping of atrial fibrillation. *J Cardiovasc Electrophysiol*. 2021;32:2393–2403. doi: [10.1111/jce.15170](https://doi.org/10.1111/jce.15170)
 34. Zaman JAB, Sauer WH, Alhussaini MI, Baykaner T, Borne RT, Kowalewski CAB, Busch S, Zei PC, Park S, Viswanathan MN, et al. Identification and characterization of sites where persistent atrial fibrillation is terminated by localized ablation. *Circ Arrhythm Electrophysiol*. 2018;11:e005258. doi: [10.1161/CIRCEP.117.005258](https://doi.org/10.1161/CIRCEP.117.005258)
 35. Lee S, Sahadevan J, Khrestian CM, Cakulev I, Markowitz A, Waldo AL. Simultaneous Batrial high-density (510–512 Electrodes) epicardial mapping of persistent and long-standing persistent atrial fibrillation in patients: new insights into the mechanism of its maintenance. *Circulation*. 2015;132:2108–2117. doi: [10.1161/CIRCULATIONAHA.115.017007](https://doi.org/10.1161/CIRCULATIONAHA.115.017007)
 36. Ip JE, Cheung JW, Chung JH, Liu CF, Thomas G, Markowitz SM, Lerman BB. Adenosine-induced atrial fibrillation: insights into mechanism. *Circ Arrhythm Electrophysiol*. 2013;6:e34–37. doi: [10.1161/CIRCEP.113.000480](https://doi.org/10.1161/CIRCEP.113.000480)
 37. Cheung JW, Lin FS, Ip JE, Bender SR, Siddiqi FK, Liu CF, Thomas G, Markowitz SM, Lerman BB. Adenosine-induced pulmonary vein ectopy as a predictor of recurrent atrial fibrillation after pulmonary vein isolation. *Circ Arrhythm Electrophysiol*. 2013;6:1066–1073. doi: [10.1161/CIRCEP.113.000796](https://doi.org/10.1161/CIRCEP.113.000796)
 38. de Groot N, van der Does L, Yaksh A, Lanters E, Teuwen C, Knops P, van de Woestijne P, Bekkers J, Kik C, Bogers AD, et al. Direct proof of endo-epicardial asynchrony of the atrial wall during atrial fibrillation in humans. *Circ Arrhythm Electrophysiol*. 2016;9. doi: [10.1161/CIRCEP.115.003648](https://doi.org/10.1161/CIRCEP.115.003648)
 39. Knecht S, Sohal M, Deisenhofer I, Albenque J-P, Arentz T, Neumann T, Cauchemez B, Duytschaever M, Ramoul K, Verbeet T, et al. Multicentre evaluation of non-invasive biatrial mapping for persistent atrial fibrillation ablation: the AFACART study. *Europace*. 2017;19:1302–1309. doi: [10.1093/europace/euw168](https://doi.org/10.1093/europace/euw168)
 40. Shi R, Parikh P, Chen Z, Angel N, Norman M, Hussain W, Butcher C, Haldar S, Jones DG, Riad O, et al. Validation of dipole density mapping during atrial fibrillation and sinus rhythm in human left atrium. *JACC Clin Electrophysiol*. 2020;6:171–181.

SUPPLEMENTAL MATERIAL

Data S1. Supplemental Methods

Propagation pattern characterisation

Propagation patterns described are identified using AcQTrack, an integrated platform within the AcQMap system. The propagation history map is first generated based on virtual dipole signals from each of approximately 3,500 vertices on the chamber surfaces and derived from biopotential signals recorded on 48 non-contact electrodes. This map allows visualisation of wavefronts over the atrial surface. AcQTrack evaluates the propagation of these wavefronts to identify specific patterns of activation. Every vertex of the chamber is continuously analysed during the display of the propagation history map thereby allowing real-time identification of regions of interest, which can be displayed as both a dynamic map (where each activation pattern is highlighted during playback of the propagation history) and a cumulative map, where a sliding scale allows adjustment to the display according to the frequency of each pattern detected at any localised site. Patterns of activation identified include focal firing (FF), localised irregular activation (LIA) and localised rotational activation (LRA), with the specific algorithm used for their detection described below. Wavefronts that do not meet these definitions (for example smooth planar wavefronts) are discounted.

Focal firing (FF)

- The focal activation algorithm determines whether an activation at a vertex came from a previous cardiac wavefront, or whether activation spontaneously started from the current activation. Focal activation is detected at a vertex if an activation is earlier than its neighbors' activation by at least 2-5 ms (default 3ms), and conduction spreads outward from the early activation.
- Activations are connected as a wavefront if the time difference between the two activation times would produce a conduction velocity greater than 0.05 m/s.

Localised irregular activation (LIA)

- The localised irregular activation algorithm computes the difference in angle between cardiac conduction entering and leaving a confined region, as illustrated in **Figure S1**. If the angle difference of conduction entering and leaving a confined region exceeds 90 degrees, localised irregular activation is detected in the region.
- An area of approximately 200-300 mm² is considered a confined region
- Wavefronts are considered to be passing through the region if the activation times differences between the border of the confined region and the central vertex would result in a conduction velocity between 0.3 m/s to 3.0 m/s.
- Activations are grouped into entering and leaving the region based on the activation time with comparison to the central vertex. A mean conduction vector entering the region and leaving the region are then computed. Angle difference between the vector entering and leaving the region are computed and if the difference exceeds 90 degrees, LIA is detected.

Localised rotational activation (LRA)

- The localised rotational activation algorithm computes the degrees of conduction propagation around a central point by summing the angle differences of sequential conduction velocity vector directions around the central point, as illustrated in **Figure S2**. If the rotational angle of conduction vector changes exceeds 270 degrees, equating to total angle of propagation change of 360 degrees, rotation is detected at the central point. An area of approximately 200-300 mm² around the central point is considered.
- To ensure smooth propagation around the central point, an r^2 of a linear fit of activation time to position around the central vertex must exceed 0.7.
- Conduction velocity vector directions changes cannot exceed 45 degrees per position change around the vertex

- Activation time difference around the central obstacle must be greater than 50ms.

Propagation pattern quantification

Quantification of these propagation patterns is required to enable comparisons. Both global measures of activation patterns across the chamber as well as methods to localise specific regions with highly repetitive activation were needed. Occurrences of these activation patterns in any given recording are often distributed widely across the chamber at low frequency with clustering of patterns at higher frequency. However, the specific frequency threshold that differentiates localised regions of most repetitive activation is highly variable between patients and maps. Whilst in one recording of a fixed duration a specified frequency threshold may be suitable, in another recording the frequency across the whole chamber may be above this threshold (as a result of different properties of AF propagation between patients/recordings) meaning that no activation occurrences are excluded and the region with the most repetitive patterns therefore not differentiated. A method that considers these observations was required allowing comparison of the statistical properties of each map obtained with the requirement to:

1. Be able to quantify global chamber occurrences to quantify “substrate properties”
2. Able to exclude infrequent occurrences that may represent false positive detections or isolated findings unlikely to be mechanistically significant
3. Identify localised regions with the most repetitively occurring patterns that may be targeted by ablation
4. Provide output according to the number of occurrences of each pattern, the proportion of time the patterns were present, and the proportion of the chamber surface area affected

A custom designed programme was developed with the aim of meeting these requirements. The process is outlined in **Figure S3**. Initially, all AcQTrack data is exported to

create a static map quantifying every pattern occurrence at each vertex of the chamber anatomy for the entire recording duration (**Figure S3A**). Each single occurrence of an activation pattern identified by AcQTrack is represented as a patch of the chamber surface that occupies all vertices within the specific confined zone (of 200-300mm²) at which the activation pattern is detected by AcQTrack (as outlined above) and for the specific period of time that the pattern remains (**Figure S3B**). The number of these unique patches equates to the number of occurrences of the specified propagation pattern (**Figure S3C**). When taken over the duration of the recording, the proportion of time in which activation patterns are detected on the chamber surface represents the time parameter (**Figure S3C**). Similarly, the proportion of the chamber in which an occurrence is detected represents the surface area affected (**Figure S3D**). Where occurrences overlapped in both space and time, potentially representing a pivot point that drifts across a region rather than remaining at a single anatomical vertex these were counted as a single occurrence (as seen in **Figure S3C**). In addition, a 5ms inclusion tolerance is included where occurrences are detected separately but within the same location less than 5ms apart. This is to ensure that an occurrence is not double counted when a short period is seen during which the AcQTrack parameters are not met but the time duration is too short to account for a separate wavefront activating that region. When this is applied to the threshold regions (described below) to quantify pattern occurrences within these zones, only patches where the centre falls within the specified zone is counted rather than any patch that purely overlaps that region.

Cut off thresholds are then applied to exclude outlying data and identify the localised regions with the most repetitive pattern occurrences. The number of occurrences in each region and the proportion of time that they are present are known. These factors are therefore used to determine the threshold. The initial static map displays all occurrences with no cut off applied (in **Figure 2** in the main paper; zero on the x axis i.e. every occurrence is counted). The percentage of the recording time with the relevant pattern is shown on the Y axis. As the cut off is increased along the X axis, i.e. only regions with increasing numbers of

occurrences are included, the proportion of time these are present decreases. A standardised cut off for the minimum absolute number of occurrences in any region does not allow for a relative correction for the varying total numbers between patients. For example where very high numbers are detected in one map with a minimum of five occurrences in any single region, then a cut off of 4 would not exclude any outlying data, compared to another map where very few detections were seen and the same cut off disproportionately excludes important data. Furthermore, an absolute cut off does not take into account the recording duration analysed. Our approach applies a threshold relative to the total time pattern occurrences are present, as illustrated in figure 2. Thresholds can then be applied that result in an exclusion of occurrences resulting in a reduction in the percentage of time that LIA is present. The highest threshold identifies the region with only the most repetitive activation pattern occurrences.

For the example used in figure 2, a colour coded representation of the number of LIA occurrences for each of the (approximately) 3500 vertices on the left atrial geometry is provided. Cut-offs were then used to eliminate the low frequency vertices, which is also those in which LIA activity was present for a relatively small proportion of the total percentage time any LIA activity was present at any part of the whole chamber. The X axis has all 3500 vertices grouped by the minimum number of individual LIA occurrences seen at that vertex during that 5-second recording. The Y axis represents the percentage of time that at least 1 of the 3500 vertices displayed LIA activity during the 5-second segment. In this example the chart indicates that for 91% of the time, any vertex which showed 1 or more LIA occurrences during the recording was exhibiting that activity (thus, for 9% of the 5 second recording there was no LIA activity at any site). To eliminate those vertices which only very infrequently displayed occurrences, a 5% cut off is introduced. This is a relative 5% of the overall percentage time that one or more occurrences were present during the recording and thus the threshold moves down from 91% to 86.5% of the overall percentage time. This has the impact of excluding those low frequency vertices which contributed very

little to the total time that one or more LIA were present, eliminating the red and most of the orange and yellow colours.

When the threshold is increased to a 10% cut-off (and drops to a total percentage time of 81.9%), this has the effect of excluding all of the vertices which had 5 or fewer LIA occurrences, eliminating more yellow and green colour-coded areas. Finally, a 20% cut off moves the threshold of percentage time LIA were present at any point on the whole chamber from 91% down to 72.8% and in doing so in this patient's recording excludes all of those vertices which displayed 8 separate LIA occurrences or fewer and the colour coding on the map is focused in on the green and dark blue areas.

What can be demonstrated in the bar chart is that the small area in purple, surrounded by dark blue, that demonstrated the most individual LIA occurrences, occupied less than 10% of the recording segment time, i.e. the 21 individual LIA occurrences occurring in those vertices had a cumulative time of less than 0.5 of a second. This is because LIA activity is a depolarisation phenomenon and will not be present during repolarisation, which takes up the majority of the cycle length. The very nature of slow, pivoting and stuttering propagation may also lead to one very disorganised wavefront being counted as multiple LIA occurrences, hence the need to incorporate percentage time as a modifier. If it was desirable to show all vertices which showed 5 or more LIA occurrences during the 5-second segment, the threshold would need to be decreased to less than 5% (i.e. no cut-off) and a much larger number of vertices would be shown across a wider colour range and percentage time of the 5 second segment

Further impetus for this approach is that there may not be a fixed relationship between the frequency of pattern occurrences and the duration that the patterns are present. Fewer occurrences may persist for longer (e.g. multiple rotations of LRA) in one recording whilst a higher frequency in another recording (e.g. short-lived pivoting LIA) may last for shorter durations. This is illustrated in figure S4. In scenarios with a high frequency of pattern occurrences and a high degree of clustering a threshold method of either a fixed percentage

of occurrences or the dynamic thresholding method explained above produce similar results (S4A). However, in examples with a less clearly delineated cluster or a lower frequency of occurrences, a fixed percentage method resulted in exclusion of areas with a high number of occurrences that persist for a longer duration and therefore may be mechanistically important (S4B, C).

Supplemental Figures

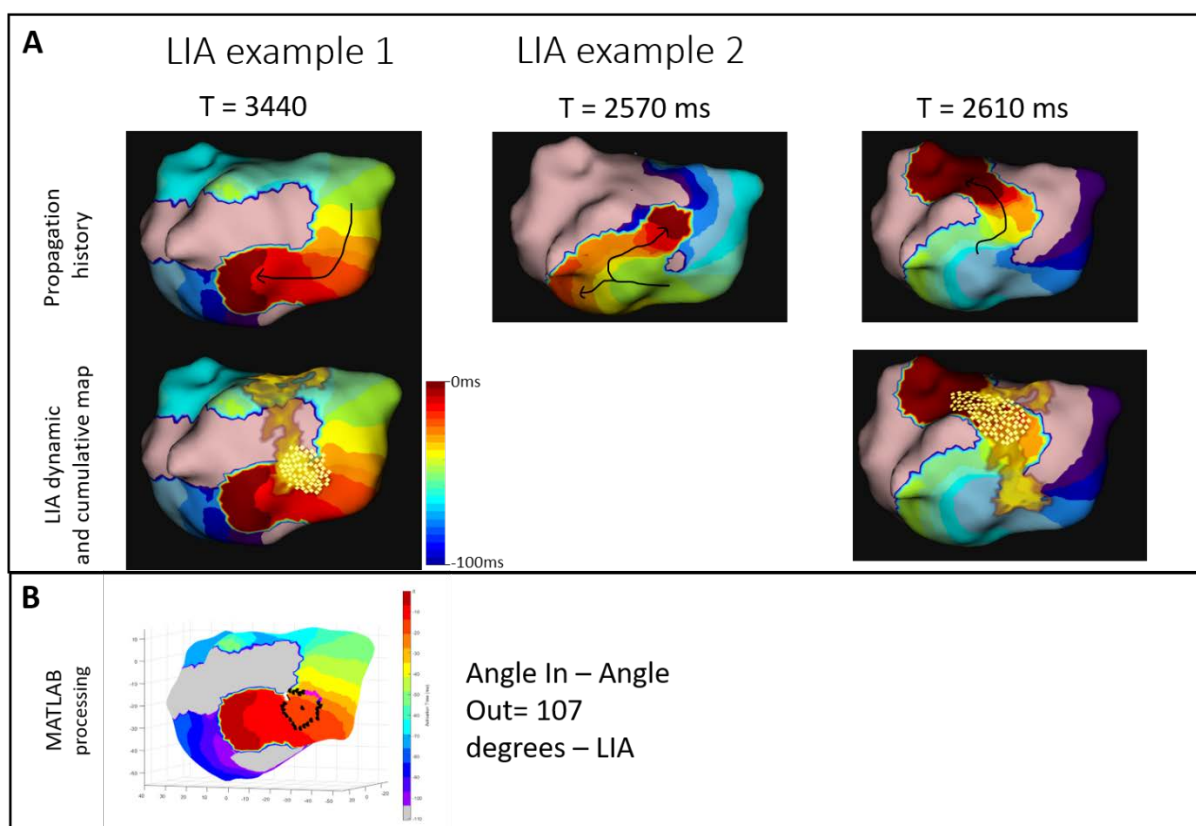


Figure S1 Examples of patterns characterised as LIA are shown in A. Top row shows static images of a propagation history map taken at 3 time points with the row below including the dynamic view of LIA detection (yellow dots) and the cumulative map (yellow patch overlay) highlighting a region over the posterior wall where a frequency of LIA above a specified (user defined) threshold was detected. Panel B illustrates the computational processing that results in LIA classification for example 1. Red denotes the leading edge of the wavefront and purple the trailing edge. The time difference used for this display can be adjusted manually (here it is set to 100ms).

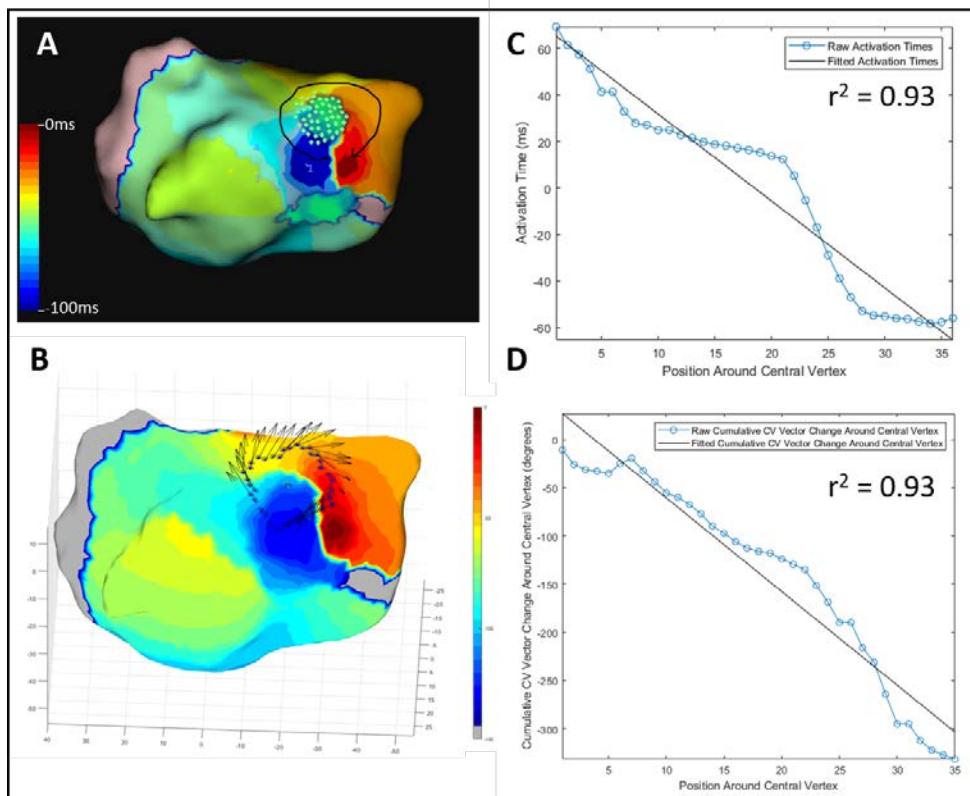


Figure S2 (A) shows a static propagation history map including the dynamic view of LRA detection (green dots) and the cumulative map (green patch overlay) highlighting a region where a frequency of LRA above a specified (user defined) threshold was detected. (B) illustrates the processing and where activation times (C) and vectors (D) are plotted at points around a central vertex within the algorithm. As in figure S1, red denotes the leading edge of the wavefront and purple the trailing edge with the time difference set to 100ms.

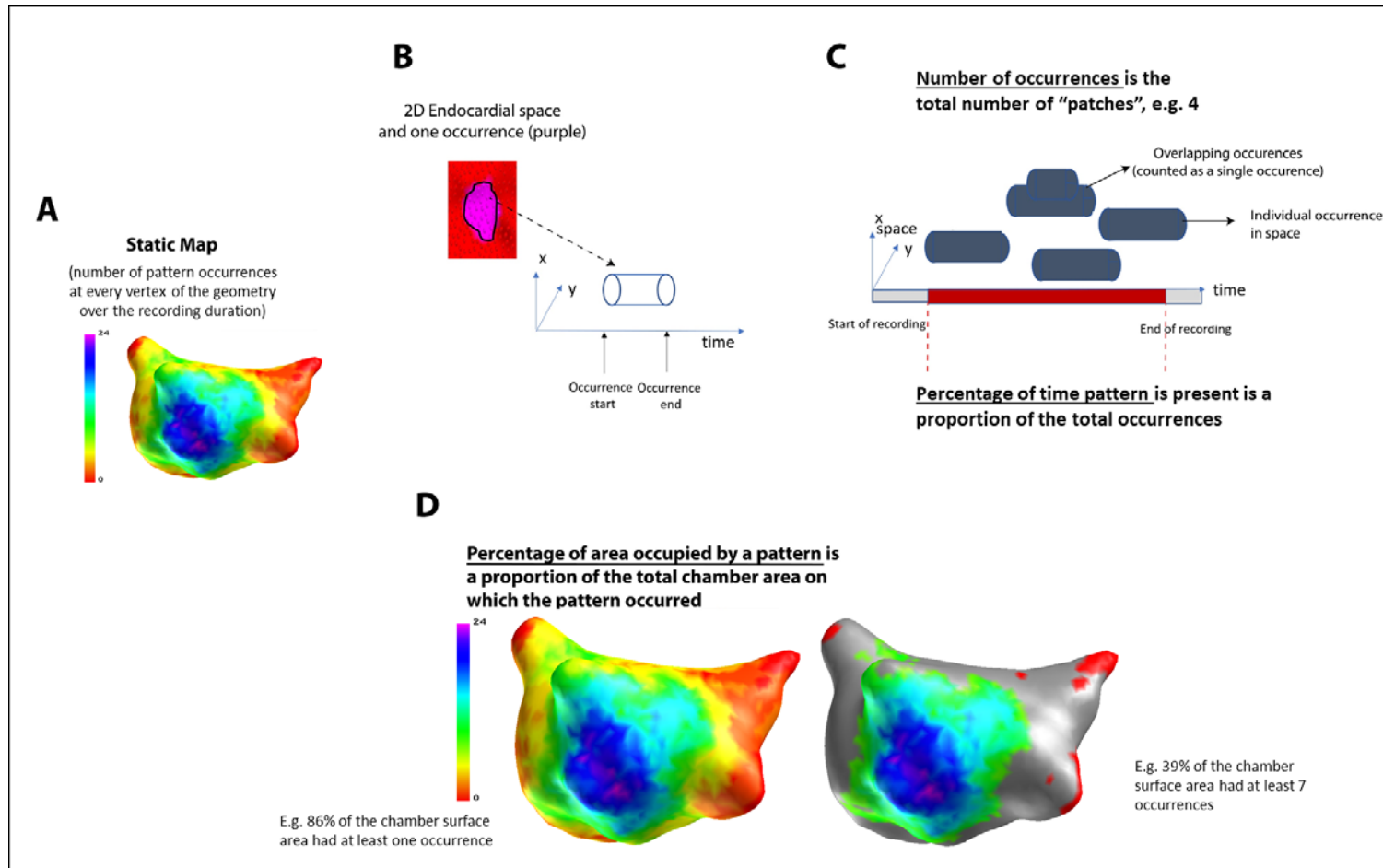


Figure S3 Method for AcQTrack pattern quantification. A static map is generated (A) demonstrating all pattern occurrences. Each occurrence is identified in space as the confined zone on the endocardial surface at which the activation pattern is detected by AcQTrack (in B shown as a purple patch on the red chamber surface and represented for illustrative purposes by a single cone) for the duration of time that the pattern remains (B) allowing calculation of the total number of occurrences and the percentage time they are present (C), as well as the proportion of the chamber surface area affected (D).

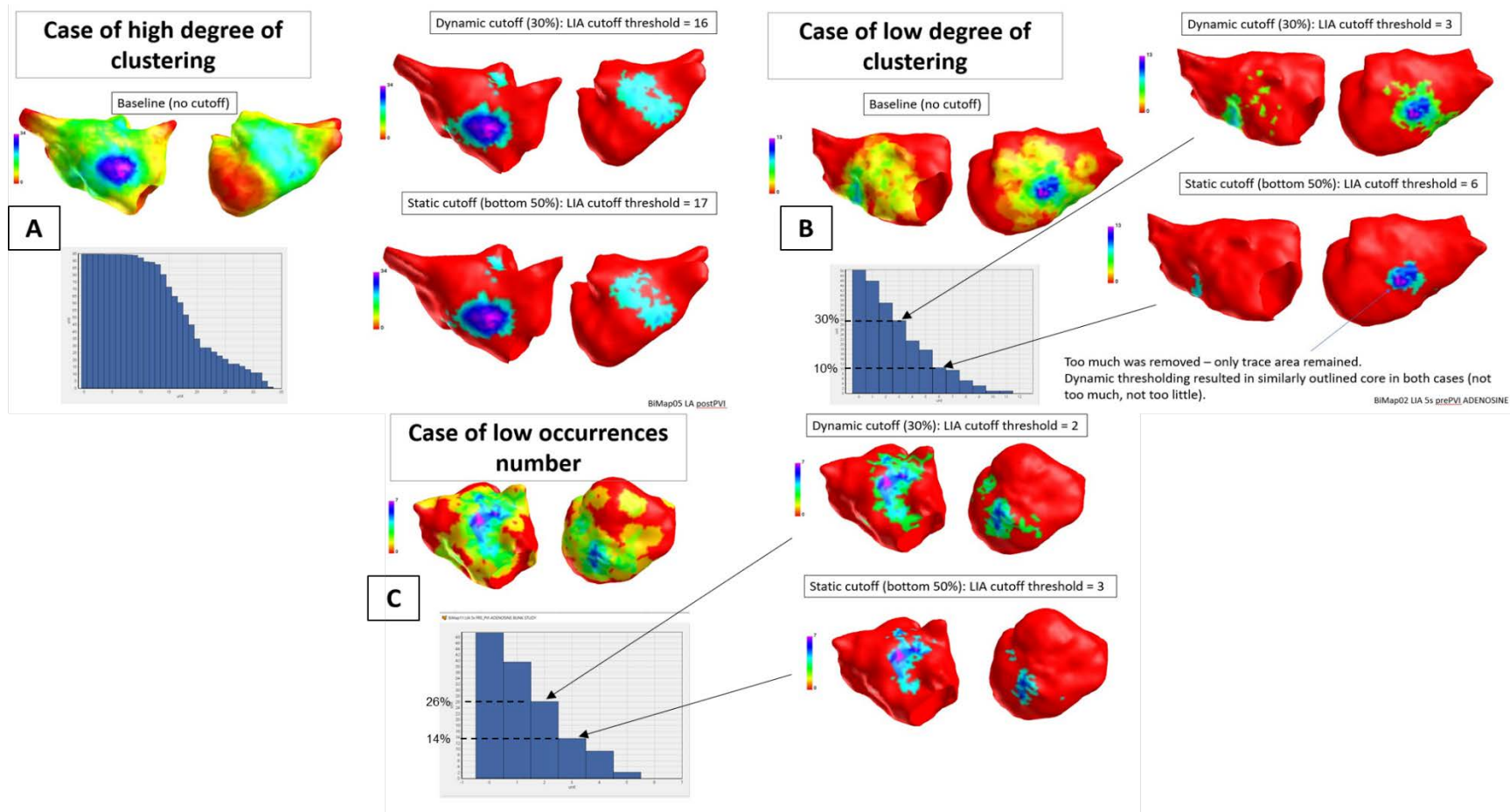


Figure S4 In a case with a high frequency of occurrences and high degree of clustering both a percentage frequency and a dynamic threshold approach produce similar results (A). However, where there is less clear clustering (B) a fixed percentage approach excludes regions where patterns occur for a significant duration i.e. exclusion is too high therefore potentially excluding areas of importance. This may also be the case in an example with a low frequency of patterns that last for a relatively longer period of time (C).

Supplemental Tables

Variable	Cut off (%)	Pre-PVI				Post-PVI				Post non-PVI ablation			
		Baseline (SD)	Adenosine (SD)	Difference (95% CI)	p value	Baseline (SD)	Adenosine (SD)	Difference (95% CI)	p value	Baseline (SD)	Adenosine (SD)	Difference (95% CI)	p value
LRA number	0	18±8.5	22.5±8.5	4.8 (-2.9 – 12.0)	0.2044	15.9±8.0	25.6±12.4	9.7 (2.0 – 17.5)	0.0173	14.2±5.8	24.0±6.3	9.8 (5.5 – 14.1)	0.0007
	5	12.9±6.7	17.1±7.3	4.2 (-1.5 – 9.9)	0.1360	11.5±7.0	20.1±10.1	8.6 (1.4 – 15.8)	0.0230	9.1±5.2	17.8±5.2	7.9 (4.4 – 12.9)	0.0016
	10	11.9±6.9	16.9±7.2	5.0 (-0.6 – 10.6)	0.0749	10.7±6.6	18.9±9.8	8.2 (1.5 – 14.8)	0.0203	9.1±5.2	17.6±5.2	8.5 (3.9 – 13.0)	0.0027
	20	8.2±6.3	13.4±4.4	5.5 (0.5 – 9.9)	0.0345	9.0±5.4	14.5±8.4	5.5 (-0.6 – 11.6)	0.0720	7.8±3.8	14.1±5.3	6.3 (1.9 – 10.8)	0.0116
	30	7.3±5.0	10.9±3.9	3.6 (-0.1 – 7.4)	0.0551	6.5±4.0	11.5±6.1	5.0 (1.3 – 8.6)	0.0118	6.9±3.4	12.3±4.3	5.4 (1.3 – 9.6)	0.0156
	40	6.5±4.4	9.3±3.3	2.8 (-0.6 – 6.0)	0.0935	4.8±2.9	10.7±5.5	5.9 (2.2 – 9.5)	0.0040	5.3±2.1	10.2±3.5	4.9 (2.9 – 6.9)	0.0005
LRA time	0	34.2±14.2	40.9±14.3	6.7 (-5.6 – 18.9)	0.2537	27.8±9.7	46.3±19.4	18.5 (6.5 – 30.3)	0.0050	27.5±11.9	41.3±8.7	13.8 (4.7 – 22.8)	0.0079
	5	28.8±13.0	34.4±13.3	5.6 (-5.3 – 16.6)	0.2810	23.4±10.1	41.3±17.9	17.9 (6.2 – 29.4)	0.0053	20.9±11.6	34.7±8.3	13.8 (5.4 – 22.3)	0.0054
	10	27.4±13.5	34.0±13.0	6.6 (-4.1 – 17.3)	0.2011	22.5±9.4	39.3±17.6	16.8 (6.0 – 27.6)	0.0048	20.9±11.6	34.3±8.2	13.4 (4.4 – 22.3)	0.0090
	20	19.8±12.5	28.8±10.5	9.0 (-2.0 – 20.0)	0.0991	19.9±9.6	32.4±16.3	12.5 (1.4 – 23.6)	0.0301	18.9±9.8	28.2±6.7	9.3 (1.2 – 17.5)	0.0297
	30	18.6±10.9	24.6±8.7	6.0 (-3.1 – 14.9)	0.1722	15.7±7.8	26.4±13.4	10.7 (3.4 – 17.9)	0.0069	17.0±9.0	25.2±6.5	8.2 (0.6 – 15.7)	0.0381
	40	17.5±10.1	21.8±7.7	4.3 (-3.6 – 12.3)	0.2491	11.9±6.0	24.7±11.9	12.8 (5.0 – 20.6)	0.0033	13.1±5.4	21.7±7.1	8.6 (4.5 – 12.8)	0.0014
LRA SA	0	25.6±8.7	28.0±10.2	2.4 (-4.9 – 9.7)	0.4776	21.1±8.0	30.9±12.2	9.8 (1.7 – 17.8)	0.0213	20.2±8.1	29.5±6.7	9.3 (5.6 – 13.0)	<0.0005
	5	16.0±6.9	15.8±7.6	-0.2 (-5.6 – 5.3)	0.9414	12.1±6.3	16.8±7.4	4.7 (-1.8 – 11.2)	0.1407	9.5±4.8	14.9±4.3	5.4 (3.3 – 7.4)	<0.0005
	10	13.5±6.2	15.5±7.7	2.0 (-3.2 – 7.8)	0.4105	10.3±4.9	14.4±6.6	4.1 (-0.9 – 9.2)	0.0990	9.5±4.8	14.3±4.1	4.8 (2.0 – 7.5)	0.0041
	20	7.7±4.1	10.9±4.1	3.2 (0.3 – 6.2)	0.0342	7.9±3.3	9.6±4.8	1.6 (-2.2 – 5.6)	0.3788	7.5±2.7	10.1±3.3	2.6 (0.6 – 4.5)	0.0162
	30	6.8±2.5	8.6±4.7	1.8 (-0.9 – 4.7)	0.1633	5.1±2.3	6.9±3.5	1.8 (-0.2 – 3.8)	0.0733	6.4±2.8	7.8±2.3	1.4 (-0.6 – 3.6)	0.1312
	40	5.8±1.9	6.8±3.1	1.0 (-0.6 – 2.6)	0.1843	3.7±2.0	6.1±3.1	2.4 (0.1 – 2.6)	0.0417	5.0±2.3	6.1±2.3	1.1 (-0.3 – 2.6)	0.1097

Table S1. Impact of adenosine of LRA frequency, duration and surface area, pre-pulmonary vein isolation, post-pulmonary vein isolation and following non-pulmonary vein ablation. LRA: Localised rotational activation; PVI: pulmonary vein isolation; SA: surface area.

Variable	Cut off (%)	Group	n	Mean	Standard deviation	p-value	95 % Confidence interval
LRA number	0	DCCV	16	16.9	7.9	0.0760	-0.8 – 13.8
		Sinus with ablation	6	10.3	5.0		
LRA percent time	0	DCCV	16	31.8	13.1	0.0970	-2.1 – 23.1
		Sinus with ablation	6	21.3	10.9		
LRA percent SA	0	DCCV	16	23.7	8.4	0.0380	0.5 – 16.6
		Sinus with ablation	6	15.1	6.8		
LRA number	5	DCCV	16	12.3	6.0	0.0590	-0.2 – 11.2
		Sinus with ablation	6	6.8	4.8		
LRA percent time	5	DCCV	16	26.8	12.2	0.0760	-1.2 – 22.1
		Sinus with ablation	6	16.3	10.0		
LRA percent SA	5	DCCV	16	14.6	7.0	0.0490	0.0 – 13.1
		Sinus with ablation	6	8.0	5.0		
LRA number	10	DCCV	16	11.1	5.8	0.1280	-1.3 – 9.8
		Sinus with ablation	6	6.8	4.8		
LRA percent time	10	DCCV	16	25.2	12.2	0.1270	-2.8 – 20.6
		Sinus with ablation	6	16.3	10.0		
LRA percent SA	10	DCCV	16	11.7	5.5	0.1690	-1.7 – 9.1
		Sinus with ablation	6	8.0	5.0		
LRA number	20	DCCV	16	9.0	5.2	0.0270	0.7 – 10.0
		Sinus with ablation	6	3.7	2.3		
LRA percent time	20	DCCV	16	20.8	10.8	0.0380	0.6 – 20.5
		Sinus with ablation	6	10.3	6.5		
LRA percent SA	20	DCCV	16	8.3	3.3	0.0080	1.3 – 7.5
		Sinus with ablation	6	3.9	2.3		
LRA number	30	DCCV	16	7.1	4.4	0.0780	-0.4 – 7.6
		Sinus with ablation	6	3.5	2.6		
LRA percent time	30	DCCV	16	17.4	9.7	0.0940	-1.4 – 16.8
		Sinus with ablation	6	9.8	7.3		
LRA percent SA	30	DCCV	16	6.1	2.5	0.0450	0.1 – 5.1
		Sinus with ablation	6	3.5	2.7		
LRA number	40	DCCV	16	6.1	4.1	0.1410	-1.0 – 6.6
		Sinus with ablation	6	3.3	2.5		
LRA percent time	40	DCCV	16	15.4	9.8	0.1740	-3.0 – 15.2
		Sinus with ablation	6	9.2	6.8		
LRA percent SA	40	DCCV	16	5.0	2.2	0.1220	-0.5 – 4.2
		Sinus with ablation	6	3.2	2.7		

Table S2. Difference in localised rotation activation frequency, duration and surface area at baseline according to acute procedural outcome.

Variable	Cut off (%)	Group	n	Mean	Standard deviation	p-value	95 % Confidence interval
LRA number	0	DCCV	16	22.7	9.1	0.738	-7.8 – 10.9
		Sinus with ablation	6	21.2	10.1		
LRA percent time	0	DCCV	16	40.7	14.5	0.971	-15.3 – 15.9
		Sinus with ablation	6	40.5	18.5		
LRA percent SA	0	DCCV	16	27.4	8.9	0.986	-10.5 – 10.3
		Sinus with ablation	6	27.5	14.1		
LRA number	5	DCCV	16	17.5	8.0	0.731	-6.6 – 9.3
		Sinus with ablation	6	16.2	7.9		
LRA percent time	5	DCCV	16	34.8	13.8	0.988	-14.3 – 14.5
		Sinus with ablation	6	34.7	16.2		
LRA percent SA	5	DCCV	16	15.1	6.0	0.943	-6.9 – 7.4
		Sinus with ablation	6	14.9	9.9		
LRA number	10	DCCV	16	16.9	7.6	0.715	-6.4 – 9.1
		Sinus with ablation	6	15.5	8.2		
LRA percent time	10	DCCV	16	34.0	13.7	0.998	-14.5 – 14.5
		Sinus with ablation	6	33.9	16.7		
LRA percent SA	10	DCCV	16	14.0	5.6	0.897	-7.6 – 6.7
		Sinus with ablation	6	14.4	10.3		
LRA number	20	DCCV	16	13.4	6.3	0.772	-5.3 – 7.1
		Sinus with ablation	6	12.5	5.8		
LRA percent time	20	DCCV	16	27.9	12.5	0.795	-14.4 – 11.2
		Sinus with ablation	6	29.6	13.7		
LRA percent SA	20	DCCV	16	10.1	4.5	0.941	-4.6 – 4.9
		Sinus with ablation	6	9.9	5.4		
LRA number	30	DCCV	16	11.2	4.9	0.388	-2.8 – 6.8
		Sinus with ablation	6	9.2	4.4		
LRA percent time	30	DCCV	16	23.2	10.0	0.88	-11.1 – 9.6
		Sinus with ablation	6	23.9	11.5		
LRA percent SA	30	DCCV	16	8.0	4.1	0.324	-2.2 – 6.2
		Sinus with ablation	6	6.0	4.4		
LRA number	40	DCCV	16	10.3	4.6	0.238	-1.9 – 7.2
		Sinus with ablation	6	7.7	4.4		
LRA percent time	40	DCCV	16	21.8	9.6	0.767	-8.6 – 11.5
		Sinus with ablation	6	20.3	11.3		
LRA percent SA	40	DCCV	16	7.0	3.0	0.126	-0.7 – 5.4
		Sinus with ablation	6	4.7	3.1		

Table S3. Difference in localised rotational activation frequency, duration and surface area following adenosine according to acute procedural outcome.